Joint Component Sizing and Energy Management for Fuel Cell Hybrid Electric Trucks

Qian Xun, *Graduate Student Member, IEEE*, Nikolce Murgovski, and Yujing Liu, *Senior Member, IEEE*

***Abstract*—This paper proposes a cost-effective way to design and operate fuel cell hybrid electric trucks (FCHETs) where a chance-constrained optimization is formulated. The aim of the introduced problem is to minimize a summation of component cost and operational cost with consideration of fuel cell (FC) degradation and cycle life of energy buffer. We propose to decompose the problem into two sub-problems that are solved by sequential convex programming. The delivered power satisfies a cumulative distribution function of the wheel power demand, while the truck can still traverse driving cycles with a similar speed and travel time without delivering unnecessarily high power. This allows to downsize powertrain components, including electric machine, FC and energy buffer. A case study considering different energy buffer technologies, including supercapacitor (SC), lithium-ion battery (LiB), and lithium-ion capacitor (LiC) is investigated in a set of trucking applications, i.e. urban delivery, regional delivery, construction, and long-haul. Results show that the power rating of the electric machine is drastically reduced when the delivered power is satisfied in a probabilistic sense. Moreover, the configuration with LiB as the energy buffer has the lowest expense but the truck with LiC can carry more payload.**

***Index Terms*—Chance-constrained, energy buffer, fuel cell hybrid electric trucks (FCHETs), sequential convex programming, wheel power demand.**

I. Introduction

HEAVY duty vehicles, and freight transport in general, are known to emit large amount of greenhouse gas (GHG) emissions. One way of reducing these emissions is by exploring energy efficient solutions, such as electrification of transportation [1]. A typical example is battery electric vehicles, which can achieve zero-emissions, but major drawbacks of limited range and long "refueling" time make them less attractive in trucking applications. Alternatively, fuel cell (FC) vehicles might be a promising solution with the superiority in high energy density and fast refueling time. Among all FC types, polymer electrolyte membrane FC (PEMFC) is proved to be commercially suitable for transportation and automotive applications, especially for passenger cars, buses, logistic vehicles, and trucks [2]. A PEMFC-powered truck, without any GHG emissions if green hydrogen is assumed, can achieve a comparable performance to a conventional internal combustion engine vehicle in terms of driving range and refueling time [3]. For example, the XCIENT Fuel Cell [4], with a travel range of about 400 km, can be charged within 8 to 20 min, depending on the ambient temperature and using a 350 bar tank with a capacity of 31 kg hydrogen.

However, a solely FC truck is prone to slow dynamics and is unable to recover regenerative energy. The hybridization of the FC with an energy storage system, e.g. supercapacitor (SC), lithium-ion battery (LiB), or a Lithium-ion capacitor (LiC), which combines advantages of both LiB and SC, is an essential way to meet the power demand and achieve required performance. Examples of commercial fuel cell hybrid electric trucks (FCHETs) are the Alpha truck [5], XCIENT Fuel Cell [6], and some other available truck models [7], [8]. Furthermore, the FC in an FCHET can be designed and operated to serve different goals, such as range extender or main power supply. In these trucks, component sizing and energy management are critical in reducing purchasing cost, increasing durability of FC stack and decreasing operational cost.

Energy management strategies for FC hybrid electric vehicles can be classified into heuristic and optimal. The heuristic-based methods are developed according to engineering experience and a series of rules, whereas the optimization-based schemes refer to solving a certain objective function subject to constraints. A fuzzy logic-based supervisory controller is implemented in [9] and [10] for FC/SC hybrid vehicles to meet the driving capability and enhance the FC performance. This method is also applied in [8] for an FC extended-range truck. In [11], a wavelet-based algorithm is used to decompose the load power into low- and high-frequency term to meet the vehicle power demand and enlarge the FC lifetime. A detailed study on energy management in FC/SC electric vehicles, especially the energy flow control, is reported in [12], and the short-term future energy demand is estimated to improve the hydrogen economy and power compliance. In [13], optimal energy management strategy is proposed based on mulltimode equivalent energy consumption method with consideration to four states of an FC hybrid electric tram, including traction, coasting, braking and station parking. A comprehensive investigation of energy management for FCHETs is presented in [14], where robustness of the control strategy, hydrogen economy and system lifetime are considered for real-world driving scenarios.

Manuscript received August 16, 2021; revised January 6, 2022; accepted February 15, 2022. Date of publication February 24, 2022; date of current version May 20, 2022. This work was supported by the Chalmers Area of Advance (Transport). The review of this article was coordinated by Dr. Mithat Kisacikoglu. *(Corresponding author: Qian Xun.)*

The authors are with the Department of Electrical Engineering, Chalmers University of Technology, 41296 Gothenburg, Sweden (e-mail: qian.xun@chalmers.se; nikolce.murgovski@chalmers.se; yujing.liu@chalmers.se).

This article has supplementary downloadable material available at http://doi.org/10.1109/TVT.2022.3154146, provided by the authors.

This article has supplementary downloadable material available at https://doi.org/10.1109/TVT.2022.3154146, provided by the authors.

Digital Object Identifier 10.1109/TVT.2022.3154146

The optimization of component sizing for FC hybrid powertrains is another factor that determines vehicle cost, performance and hydrogen consumption. In [15], an optimal sizing methodology is proposed where SC and different battery technologies are investigated in terms of weight, volume, cost and hydrogen consumption for an FC electric vehicle. Optimal sizing of a plug-in FC hybrid city bus is performed based on charge depleting and charge sustaining strategy in [16]. Component sizes and hydrogen consumption are estimated in [17] for FCHETs with an equivalent performance as diesel trucks. Moreover, [18] develops an optimum component sizing algorithm for FC/battery hybrid powertrains in class 4 delivery trucks and class 8 line-haul trucks to minimize relevant ownership cost. Energy sources are sized in [19] for an FC-based garbage truck using a statistical description of real-world driving data. In addition to the optimization of power sources in hybrid vehicles, electric drivetrain is optimized for a fleet of trucks using particle swarm algorithm with consideration of degrees of electrical machine commonality [20].

In some cases, component sizing and energy management are addressed at the same time to further optimize FC hybrid electric vehicles. Dynamic programming is applied in [21]–[23] to find optimal SC size and control strategies in a combined optimization of component sizing and energy management for an FC hybrid electric bus. In [24], a two-loop framework based on Pareto optimization is presented in combination with dynamic programming to solve a multi-objective optimization problem for an FC hybrid electric bus. Convex optimization has been performed in [25]–[27] for optimization of component sizing and energy management of FC electric buses hybridized with SC, battery, or both. Convex programming has also been used in [28] to optimize component sizing and energy management for an FC urban logistics vehicle. In [29], integrated design and control optimization is performed for an FC powered mining truck to minimize lifecycle cost. In [3], powertrain topologies, layout optimization, energy management strategies, and co-design optimization are summarized and reviewed.

Energy management and component sizing of FC hybrid electric vehicles have been separately or sequentially optimized in heavy-duty applications, including buses, trams and trucks. However, their combined optimization has only been well addressed in FC hybrid electric buses [25]–[27] and has not been comprehensively studied for trucking applications. To bridge this research gap, this paper presents a joint component sizing and energy management framework via convex optimization for FCHETs. Key contributions are listed as follows:

- A chance-constrained optimization problem is formulated for component sizing of electric machine, FC, and energy buffer, together with the energy management between FC and energy buffer along typical driving cycles. The proposed problem minimizes a summation of component cost and operational cost for a set of trucking applications, including urban delivery, regional delivery, construction, and long-haul.

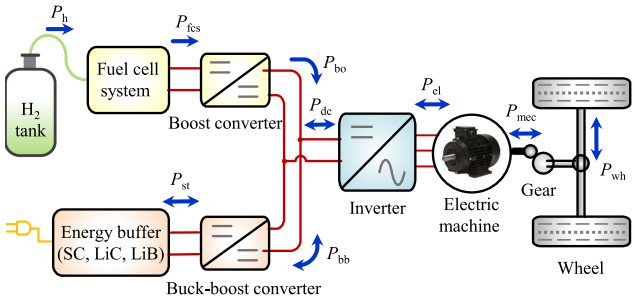

SC: supercapacitor; LiC: li-ion capacitor; LiB: Li-ion battery.

Fig. 1. Architecture of an FCHET propulsion system.

- We propose decomposing the problem into two sub-problems. Convex modeling steps are provided to effectively solve each sub-problem by sequential convex programming.
- Powertrain components are sized to satisfy wheel power demand with a user provided probability. This allows downsizing the components by not delivering unnecessarily high power, while ensuring a similar speed and travel time as those requested by specific driving cycles.
- The component sizing and energy management are conducted together where three energy buffer technologies, including SC, LiC, and LiB are investigated. The FC degradation and cycle life of the energy buffer technologies have also been taken into account.

The remainder of the paper is organized as follows. Section II presents the system architecture and component models of an FCHET in detail. The introduced optimization problem is formulated in Section III and optimization method is described in Section IV. A case study and simulation results are discussed in Section V and followed by conclusions summarized in Section VI.

II. Modeling of FCHET Powertrain

We consider a fully active hybrid architecture, with two DC/DC converters connected to the FC and the energy buffer, as shown in Fig. 1. This architecture allows full controllability of the power allocation between the FC and the energy buffer (SC, LiC, and LiB). For more details see [30]–[32]. To better utilize the energy capacity of the energy buffer, the adopted FCHET is considered as a plug-in type. The wheel power is provided by an electric machine through a differential gear. The electric machine can also operate as a generator to recover the regenerative braking energy. A three-phase inverter is connected between DC/DC converters and the electric machine to achieve power conversion between DC and AC. At the DC-side, the FC provides power through a boost converter. An energy buffer i.e. a SC, a LiC or a LiB, delivers or receives power via a buck-boost converter.

The electrical power, which is consumed by driving wheels, is provided by the FC and the energy buffer. Therefore, the power

balance equation can be deduced as

$$P_{\mathrm{wh}}(t) + P_{\mathrm{loss,em}}(t) + P_{\mathrm{aux}}(t) = \min\left(P_{\mathrm{st}}(t)\eta_{\mathrm{bb}}, \frac{P_{\mathrm{st}}(t)}{\eta_{\mathrm{bb}}}\right) + P_{\mathrm{fcs}}(t)\eta_{\mathrm{bo}}, \quad (1)$$

where $P_{\mathrm{wh}}(t) = F_{\mathrm{wh}}(t)v(t)$ is the demanded wheel power, $F_{\mathrm{wh}}(t)$ is the demanded wheel force and $v(t)$ is the desired truck speed, usually given as a driving cycle speed profile. The term $P_{\mathrm{loss,em}}(t)$ is the power losses of the drivetrain system, including the final gear, the electric machine, and the inverter, $P_{\mathrm{aux}}(t)$ is the auxiliary power during the truck movement, $P_{\mathrm{st}}(t)$ is the terminal power of the energy buffer, $P_{\mathrm{fcs}}(t)$ is the FC power, and η_{bo} and η_{bb} are the efficiencies of the boost converter and buck-boost converter, respectively. The $\min$ function ensures that η_{bb} multiplies P_{st} when P_{st} is positive, and divides otherwise.

A. Driving Cycle Specifications

Four driving cycles are considered, which consist of road altitudes and speed profiles varying along travelled distance. They represent urban delivery, regional delivery, construction, and long-haul cycles for trucks, which are developed by the European association of car manufacturers (ACEA). The maximum acceleration and deceleration are defined as $2\,\mathrm{m/s^2}$ and $-1\,\mathrm{m/s^2}$, respectively. The total traveling length for all driving cycles is around $100\,\mathrm{km}$. The driving cycles, including the cumulative distribution function (CDF) of their corresponding accelerations, are illustrated in Fig. 2. The urban delivery cycle has the lowest average speed but includes most frequent accelerations and decelerations, whereas the long-haul cycle has the highest and relatively constant average speed.

B. Longitudinal Vehicle Dynamics

The truck is considered to be a rigid body, where the total mass is assumed to be constant, set to the maximum allowed value. According to the Newton's law of motion, the demanded wheel force can be written as

$$F_{\mathrm{wh}}(t) = (m_{\mathrm{trk}} + m_{\mathrm{r}})\dot{v}(t) + \frac{\rho_{\mathrm{a}}}{2}C_{\mathrm{d}}A_{\mathrm{f}}v^2(t) + C_{\mathrm{r}}m_{\mathrm{trk}}g\cos\alpha(t) + m_{\mathrm{trk}}g\sin\alpha(t), \quad (2)$$

where m_{trk} is the total truck mass including payload, m_{r} is the equivalent mass of all rotational parts, $\rho_{\mathrm{a}}, C_{\mathrm{d}}, A_{\mathrm{f}}, C_{\mathrm{r}}, g$ and $\alpha(t)$ are the air density, drag coefficient, front area, rolling resistance coefficient, gravitational constant, and road slope, respectively.

The total truck mass consists of three parts and the mass balance is described as

$$m_{\mathrm{trk}} = x_{\mathrm{fc}}m_{\mathrm{fc}} + x_{\mathrm{s}}m_{\mathrm{s}} + m_0, \quad (3)$$

where x_{fc} and x_{s} are the scaling factors of the FC system and the energy buffer. The terms m_{fc} and m_{s} are the baseline mass of the FC system and the energy buffer with the associated DC/DC converters, respectively. The term m_0 is the mass of the remaining parts, which is a function of decision variables for a constant truck mass. The equivalent mass of the rotational parts can be written as

$$m_{\mathrm{r}} = \frac{1}{r_{\mathrm{wh}}^2}\left(k_{\mathrm{gr}}^2 J_{\mathrm{em}}x_{\mathrm{em}} + J_{\mathrm{wh}}\right), \quad (4)$$

where r_{wh} is the wheel radius, k_{gr} is the gear ratio, x_{em} is the scaling factor of the electric machine, and J_{em} and J_{wh} are the inertia of the baseline electric machine and all wheels, respectively. We denote $J_{\mathrm{trk}} = k_{\mathrm{gr}}^2 J_{\mathrm{em}}x_{\mathrm{em}} + J_{\mathrm{wh}}$.

According to (2), the demanded torque on the shaft between the electric machine and the final gear can be derived in (5) when a lossless gear is assumed,

$$T_{\mathrm{dem}}(t) = \frac{r_{\mathrm{wh}}}{k_{\mathrm{gr}}}F_{\mathrm{wh}}(t). \quad (5)$$

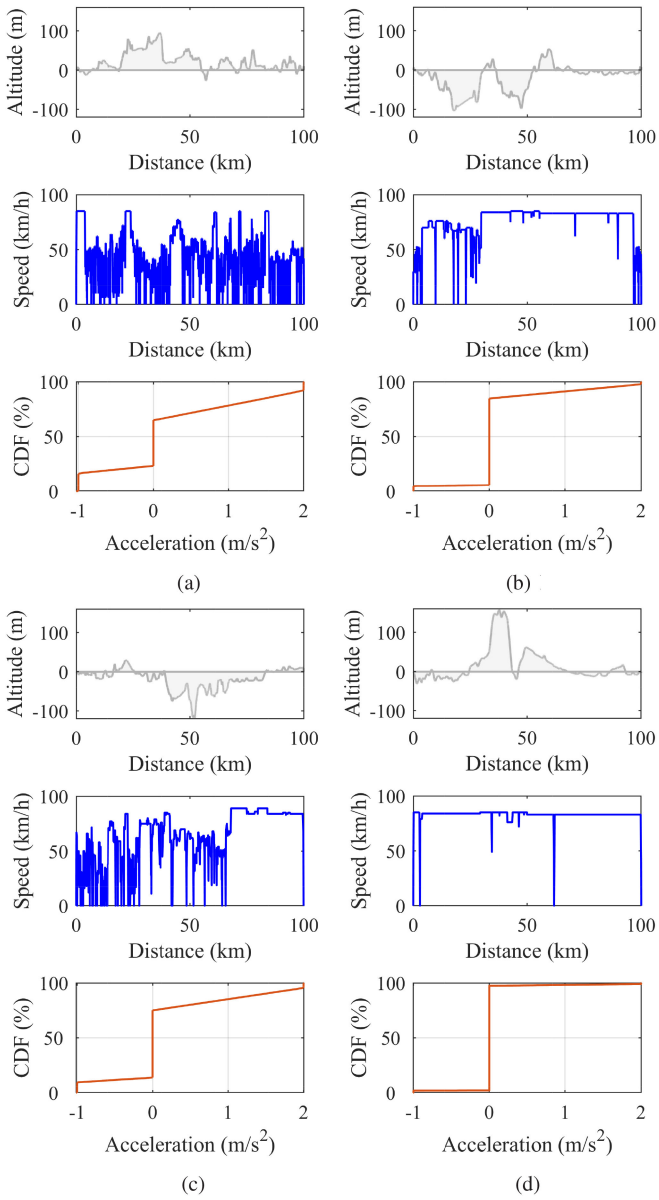

Fig. 2. Typical driving cycles and CDF of their acceleration sampled at every 1 s. (a) Urban delivery cycle. (b) Regional delivery cycle. (c) Construction cycle. (d) Long-haul cycle.

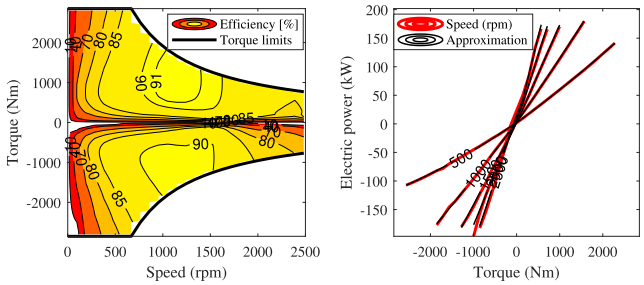

(a) (b)

Fig. 3. Efficiency map and approximation model of the electric machine with the associated inverter. (a) Efficiency map. (b) Approximation model.

Therefore, the wheel power demand can also be written as

$$P_{\mathrm{wh}}(t) = T_{\mathrm{dem}}(t)\omega(t), \tag{6}$$

where ω is the rotational speed of the electric machine.

C. Electric Drive System

A permanent magnet synchronous electric machine, with peak power of 200 kW, peak torque of 2850 Nm and peak speed of 2500 rpm, respectively, is used as a baseline in this case study. The power loss of the baseline electric machine, including losses of associated three-phase inverter, can be expressed as a quadratic function of electromagnetic torque T_{emb},

$$P_{\mathrm{loss,emb}}(\omega(t),t) = a_0(\omega(t))T^2_{\mathrm{emb}}(t) + a_1(\omega(t))T_{\mathrm{emb}}(t) + a_2(\omega(t)), \tag{7}$$

where a_0, a_1 and a_2 are speed-dependent parameters. Here, a_0 is non-negative, which guarantees that the loss model is convex in T_{emb} [33]–[35]. Therefore, the electrical power at the DC-side of the three-phase inverter is also a quadratic function of the torque. The efficiency map of the baseline electric machine with the associated inverter is shown in Fig. 3(a), and the approximated model and the measured data is shown in Fig. 3(b).

To meet the power demand of different driving cycles and various types of trucks, the electric machine can be scaled with a proper scaling factor x_{em}. The power loss of the scaled electric machine with the associated inverter can be derived as

$$P_{\mathrm{loss,em}}(t) = P_{\mathrm{loss,emb}}(t)x_{\mathrm{em}}. \tag{8}$$

By substituting $T_{\mathrm{em}}(t) = T_{\mathrm{emb}}(t)x_{\mathrm{em}}$ into (7), (8) can be rewritten as

$$P_{\mathrm{loss,em}}(t) = a_0(\omega(t))\frac{T^2_{\mathrm{em}}(t)}{x_{\mathrm{em}}} + a_1(\omega(t))T_{\mathrm{em}}(t) + a_2(\omega(t))x_{\mathrm{em}}. \tag{9}$$

The torque balance can be written as

$$T_{\mathrm{em}} = T_{\mathrm{dem}}(t) + T_{\mathrm{brk}}(t), \tag{10}$$

where T_{brk} is the dissipated torque due to mechanical braking. Electromagnetic torque is constrained as

$$T_{\mathrm{emb,min}}(\omega(t))x_{\mathrm{em}} \leqslant T_{\mathrm{em}}(t) \leqslant T_{\mathrm{emb,max}}(\omega(t))x_{\mathrm{em}}, \tag{11}$$

where $T_{\mathrm{emb,min}}$ and $T_{\mathrm{emb,max}}$ are the minimal and maximal torque limits of the baseline electric machine. The torque limits are functions of the rotational speed.

D. Fuel Cell System

1) Hydrogen Consumption Model: The PEMFC is an electrochemical energy conversion device that converts chemical energy directly into electrical energy. A baseline FC system model with power rating of $P_{\mathrm{fcb,max}} = 50\,\mathrm{kW}$ is obtained from the Advanced Vehicle Simulator (ADVISOR) software (labeled as FCANL_50H2). The system conversion efficiency of the baseline model is illustrated in Fig. 4(a), which shows that the peak efficiency of 60% is achieved at around 20 kW. Let $P_{\mathrm{fcb}}(t)$ denote the power of the baseline FC system that is limited within

$$0 \leqslant P_{\mathrm{fcb}}(t) \leqslant P_{\mathrm{fcb,max}}. \tag{12}$$

Now, let

$$P_{\mathrm{fcs}}(t) = P_{\mathrm{fcb}}(t)x_{\mathrm{fc}} \tag{13}$$

be the scaled power of FCANL_50H2. Clearly, the power limit will now translate to

$$0 \leqslant P_{\mathrm{fcs}}(t) \leqslant P_{\mathrm{fcb,max}}x_{\mathrm{fc}}, \tag{14}$$

with $x_{\mathrm{fc,min}} \leqslant x_{\mathrm{fc}} \leqslant x_{\mathrm{fc,max}}$, where $x_{\mathrm{fc,min}}$ should be greater than 0.

The consumed hydrogen of the baseline FC model, P_{hb}, can be approximated as a quadratic function of the electrical power,

$$P_{\mathrm{hb}}(t) = b_0P^2_{\mathrm{fcb}}(t) + b_1P_{\mathrm{fcb}}(t) + b_2, \tag{15}$$

where $b_j \geqslant 0, j \in \{0,2\}$. The efficiency map of the baseline FC system and the corresponded approximated model are shown in Fig. 4(b). It can be seen that the fitted quadratic function captures the hydrogen consumption of the FC system with high accuracy. Similar quadratic model has also been used for system-level powertrain analysis in [25], [27].

Let

$$P_{\mathrm{h}}(t) = P_{\mathrm{hb}}(t)x_{\mathrm{fc}} \tag{16}$$

be the hydrogen consumption of the scaled FC system. By substitution of (13) and (16) into (15), hydrogen consumption in the scaled model can be written as

$$P_{\mathrm{h}}(t) = b_0\frac{P^2_{\mathrm{fcs}}(t)}{x_{\mathrm{fc}}} + b_1P_{\mathrm{fcs}}(t) + b_2x_{\mathrm{fc}}. \tag{17}$$

2) Degradation Model: During the FC operation, a degradation takes place, the rate of which depends on internal conditions, such as temperature, pressure, membrane water content, etc. Membrane electrode assembly degradation, which is mainly due to the fading of catalyst layer [36], proton exchange membrane [37] and gas diffusion layer [38], is recognised as the main factor that influences performance and lifetime [39]–[41]. This kind of degradation is closely determined by the load profile that is often classified into 5 categories [22], [42], [43], including constant load current, current cycling, extra-low current, extra-high current and open-circuit voltage. The state of the FC degradation is therefore simply characterized as the summation of the voltage degradation rate under each load profile. This

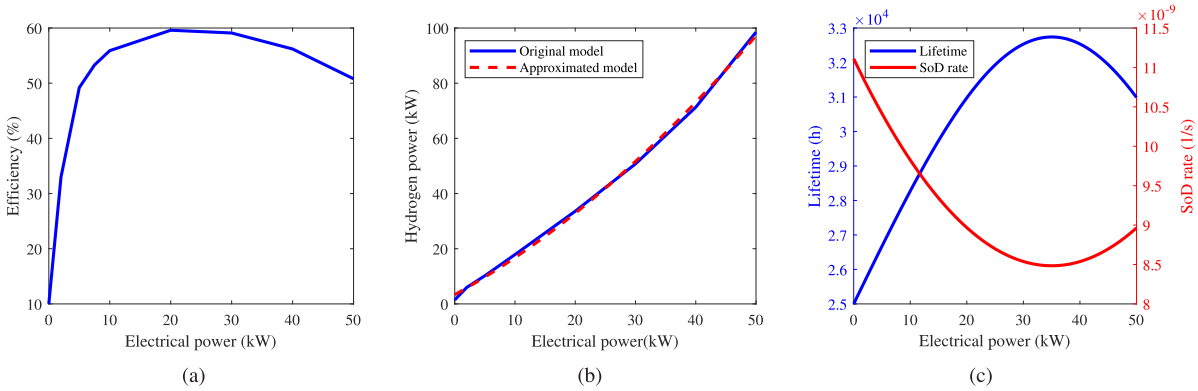

Fig. 4. Quasi-static fuel cell system modeling. (a) Efficiency map of the original model. (b) Approximation on hydrogen consumption. (c) State of degradation with respect to power.

model is usually used for statistical analysis of different load conditions.

FC degradation in terms of insufficient humidification with gas starvation or flooding problems, occurs mainly due to large power variation $\dot{P}_{\rm fcs}(t)$. To reduce such degradation, $\dot{P}_{\rm fcs}(t)$ is bounded within a certain range, typically between 2% and 20% of maximum power per second [12]. In this work, a limit of $\pm 10\,\%$ is adopted.

The FC is considered as always in "ON" state and thus the start/stop-cycle-based degradation is ignored. To prevent the FC system operating at relatively low and high power, the state of degradation (SoD) in the baseline model at time instance t is defined as the integration of the degradation rate over time [44], [45]. This is mathematically expressed as

$$\mathrm{sod}_{\rm b}(t) = \int_0^t \dot{\mathrm{sod}}_{\rm b}(\tau)\mathrm{d}\tau, \tag{18}$$

where $\dot{\mathrm{sod}}_{\rm b}(t)$ is the degradation rate that is defined as a quadratic function determined by the FC operation power in a baseline model, which can be described as

$$\dot{\mathrm{sod}}_{\rm b}(t) = d_0\left(\frac{P_{\rm fcs}(t)}{x_{\rm fc}}\right)^2 + d_1\frac{P_{\rm fcs}(t)}{x_{\rm fc}} + d_2, \tag{19}$$

where $d_j \geqslant 0, j \in \{0, 2\}$. This is depicted in Fig. 4(c), showing FC lifetime of at least 25000 hours according to the 2030 target for long-haul trucks. It can be seen that the fading rate of the SoD is greater when the FC operates at high or low power.

The SoD increasement over one driving cycle in a scaled model is constrained by

$$\mathrm{sod}(t_{\rm f}) - \mathrm{sod}(0) \leqslant \Delta\mathrm{sod}, \tag{20}$$

with $\Delta\mathrm{sod} = \dfrac{s_{\rm f}}{L_{\rm a}y_{\rm trk}}\mathrm{sod}_{\max}$, where $s_{\rm f}$ is the length of the driving cycle, $L_{\rm a}$ is the average travel distance per year, $y_{\rm trk}$ is the truck service years, and $\mathrm{sod}_{\max}$ is the maximum allowed degradation during its lifetime, which is usually set to 1. Notice that the degradation rate in a scaled FC model is assumed to be the same as that in the baseline model.

TABLE I
SPECIFICATIONS OF SC, LIC, AND LIB

	SC	LiC	LiB
Rated voltage (V)	2.7	3.5	2.3
Rated capacitance/capacity (F/As)	3000	28000	72000
Max. charge/discharge current (A)	-210/ 210	-150/ 150	-100/ 100
Internal resistance (Ω)	2.9×10^{-4}	3.5×10^{-4}	8.9×10^{-4}
Cycle lifetime (cycles)	1 000 000	1 000 000	15 000
Minimal SoC (%)	50	20	30
Maximal SoC (%)	95	90	80
Cell mass (kg)	0.51	0.83	0.52
Power density (W/kg)	5900	-	2200
Energy density (Wh/kg)	6	26	86

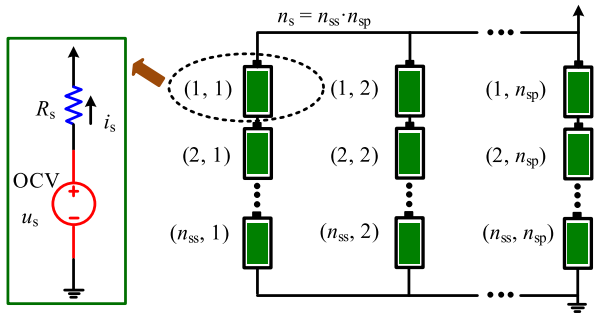

Fig. 5. Pack configuration of the energy buffer with $n_{\rm ss}$ cells connected in each string and $n_{\rm sp}$ strings connected in the pack.

E. Energy Buffer

Different energy buffer technologies, including SCs, LiCs and LiBs, are examined in this study. For the respective technologies, the cells Maxwell BCAP3000, Aowei UCK42V28000, and Toshba SCiB20Ah are selected for the investigation, with their main parameters listed in Table I. The cells are modelled as a series connection of a resistor, $R_{\rm s}$, and an open circuit voltage (OCV), $u_{\rm s}$. The baseline model of energy buffer packs consists of several strings in parallel, with each string containing the same number of cells connected in series, as shown in Fig. 5, where $i_{\rm s}$ is the cell current, $n_{\rm s}$, $n_{\rm ss}$ and $n_{\rm sp}$ are the total numbers

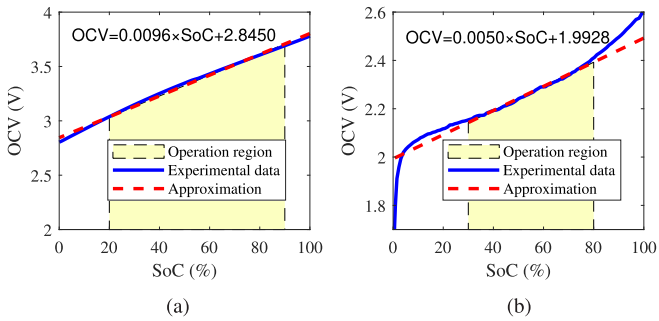

Fig. 6. OCV model of LiC and LiB with respect to the SoC levle. (a) UCK42V28000 cell. (b) Toshba 20 Ah lithium titanate battery [48].

of the cells in the pack, number of series connected cells in a string and number of parallel connected strings, respectively.

Following the model by [27], [46], a linear approximation of the OCV of each technology can be uniformly presented as

$$u_{\mathrm{s}}(t) = \frac{Q_{\mathrm{s}}}{C_{\mathrm{s}}}\mathrm{soc}_{\mathrm{s}}(t) + u_{0\mathrm{s}}, \tag{21}$$

where Q_{s}, C_{s}, $\mathrm{soc}_{\mathrm{s}}$ and $u_{0\mathrm{s}}$ represent the rated capacity, rated capacitance, state of charge (SoC) and the initial voltage of the single cell. It should be noted that for SCs, the OCV changes linearly with the SoC level and that $u_{0\mathrm{s}} = 0$. The LiC and LiB have non-zero minimum operation voltage, and linear approximations are implemented to fit the relationship between the OCV and the recommended SoC level, as shown in Fig. 6. The terminal pack power can be calculated as

$$P_{\mathrm{stb}}(t) = \left(u_{\mathrm{s}}(t)i_{\mathrm{s}}(t) - R_{\mathrm{s}}i_{\mathrm{s}}^2(t)\right)n_{\mathrm{s}}, \tag{22}$$

and the associated pack energy can be derived as

$$\begin{aligned} E_{\mathrm{sb}}(t) &= n_{\mathrm{s}}Q_{\mathrm{s}}\int_0^{\mathrm{soc_s}(t)}\left(\frac{Q_{\mathrm{s}}}{C_{\mathrm{s}}}\mathrm{soc}_{\mathrm{s}}(\tau) + u_{0\mathrm{s}}\right)\mathrm{d}\mathrm{soc}_{\mathrm{s}}(\tau) \\ &= \frac{n_{\mathrm{s}}C_{\mathrm{s}}}{2}\left(u_{\mathrm{s}}^2(t) - u_{0\mathrm{s}}^2\right). \end{aligned} \tag{23}$$

By substitution of (23) into (22), the terminal pack power can be rewritten as

$$\begin{aligned} P_{\mathrm{stb}}(t) &= P_{\mathrm{sb}}(t) - \left(\frac{P_{\mathrm{sb}}(t)}{n_{\mathrm{ss}}u_{\mathrm{s}}(t)}\right)^2 \cdot \frac{n_{\mathrm{ss}}R_{\mathrm{s}}}{n_{\mathrm{sp}}} \\ &= P_{\mathrm{sb}}(t) - \frac{R_{\mathrm{s}}C_{\mathrm{s}}P_{\mathrm{sb}}^2(t)}{2E_{\mathrm{sb}}(t) + u_{0\mathrm{s}}^2C_{\mathrm{s}}n_{\mathrm{s}}}. \end{aligned} \tag{24}$$

It can be seen that the pack energy and power are only dependent on the total number of cells and are not affected by the connection pattern. The pack dynamics is given as $\dot{E}_{\mathrm{sb}}(t) = -P_{\mathrm{sb}}(t)$ where a positive power indicates that discharging current is applied to the energy buffer. The targeted energy buffer is a scaled version of the pack shown in Fig. 5 with n_{s} known a priory. The scaling factor x_{s} should satisfy

$$x_{\mathrm{s,min}} \leqslant x_{\mathrm{s}} \leqslant x_{\mathrm{s,max}}, \tag{25}$$

where $x_{\mathrm{s,min}}$ should be greater than 0.

When scaling the energy buffer, the targeted pack energy and power can be expressed as $E_{\mathrm{s}} = x_{\mathrm{s}}E_{\mathrm{sb}}$ and $P_{\mathrm{s}} = x_{\mathrm{s}}P_{\mathrm{sb}}$, respectively. Due to the physical limitation of the SoC level and the operation current for a single cell, the internal energy and power of the target pack during the operation need to be restricted to a safe range, which can be described as

$$\begin{aligned} &\frac{x_{\mathrm{s}}n_{\mathrm{s}}C_{\mathrm{s}}}{2}\left(u_{\mathrm{s}}^2(\mathrm{soc_{s,min}}) - u_{0\mathrm{s}}^2\right) \leqslant E_{\mathrm{s}}(t) \\ &\leqslant \frac{x_{\mathrm{s}}n_{\mathrm{s}}C_{\mathrm{s}}}{2}\left(u_{\mathrm{s}}^2(\mathrm{soc_{s,max}}) - u_{0\mathrm{s}}^2\right), \\ &i_{\mathrm{s,min}}\sqrt{x_{\mathrm{s}}n_{\mathrm{s}}\left(\frac{2E_{\mathrm{s}}(t)}{C_{\mathrm{s}}} + x_{\mathrm{s}}n_{\mathrm{s}}u_{0\mathrm{s}}^2\right)} \leqslant P_{\mathrm{s}}(t) \\ &\leqslant i_{\mathrm{s,max}}\sqrt{x_{\mathrm{s}}n_{\mathrm{s}}\left(\frac{2E_{\mathrm{s}}(t)}{C_{\mathrm{s}}} + x_{\mathrm{s}}n_{\mathrm{s}}u_{0\mathrm{s}}^2\right)}, \end{aligned} \tag{26}$$

where $\mathrm{soc_{s,min}}$ and $\mathrm{soc_{s,max}}$ are the minimal and maximal SoC of the cell while $i_{\mathrm{s,min}}$ and $i_{\mathrm{s,max}}$ denote the maximal charge and discharge current, respectively. Apparently, the following equations hold, $0 \leqslant \mathrm{soc_{s,min}} \leqslant \mathrm{soc_{s,max}}$ and $i_{\mathrm{s,min}} \leqslant 0 \leqslant i_{\mathrm{s,max}}$.

Additionally, to easily compare the investigated energy buffer technologies, the cycle life of the energy buffers is used as the evaluation index for the degradation. The energy throughput during their cycle lifetime is distributed evenly between each driving cycle. Therefore, the energy throughput for a given driving cycle should satisfy

$$\int_0^{t_{\mathrm{f}}} |P_{\mathrm{s}}(t)|\,\mathrm{d}t \leqslant \frac{2N_{\mathrm{cl}}x_{\mathrm{s}}n_{\mathrm{s}}E_{\mathrm{cl}}s_{\mathrm{f}}}{y_{\mathrm{trk}}L_{\mathrm{a}}}, \tag{27}$$

where N_{cl} is the number of cycles in a whole lifetime and E_{cl} is the maximum allowable energy change per cell.

III. Problem Formulation

The introduced optimization problem is aiming to find the optimal capacity of the FC and the energy buffer, optimal power rating of the electric machine and the optimal power allocation between the FC and the energy buffer, such that the truck can traverse the driving cycle with a similar speed and travel time to those demanded. The performance metrics of trucks considered in this paper include total cost, driving range with one-time refueling, average service time, annual travel distance, acceleration characteristics, and typical driving cycle performance. The FC degradation and cycle life constraint of energy buffers are also considered, which are included into the capital cost of FC and energy buffers.

A. Objective Function

The optimization objective is formulated to minimize a cost function J, consisting of operational cost and component cost over the pre-defined driving cycle. It can be described as

$$J = C_{\mathrm{H2}} + C_{\mathrm{ele}} + C_{\mathrm{fcs}} + C_{\mathrm{eb}} + C_{\mathrm{em}}, \tag{28}$$

where C_{H2}, C_{ele}, C_{fcs}, C_{eb} and C_{em} are the cost of hydrogen consumption, electricity consumption, FC system, energy buffer and electric machine, respectively. To make the costs comparable, each cost is normalized in euros per km. Therefore, the

hydrogen cost is written as

$$C_{\mathrm{H2}} = \frac{\beta_{\mathrm{h}}}{L_{\mathrm{dc}} C_{\mathrm{h}}} \int_0^{t_{\mathrm{f}}} P_{\mathrm{h}} \mathrm{d}t, \tag{29}$$

with β_{h} being the hydrogen cost per kg and C_{h} being the lower heating value of hydrogen in J/kg. The electricity cost is written as

$$C_{\mathrm{ele}} = \frac{\beta_{\mathrm{ele}}}{L_{\mathrm{dc}}} (E_{\mathrm{s}}(0) - E_{\mathrm{s}}(t_{\mathrm{f}})), \tag{30}$$

with β_{ele} being the unit price of electricity, $E_{\mathrm{s}}(0)$ and $E_{\mathrm{s}}(t_{\mathrm{f}})$ being the stored energy of energy buffer at the beginning and the end of a driving cycle, respectively. The energy change during a travel range L_{range}, typically in the order of 600-800 km, should be limited to the maximum stored energy. As a driving cycle has shorter length than L_{range}, we assume that this energy change is evenly distributed into each driving cycle. Therefore, the energy change over one driving cycle should satisfy

$$-\frac{s_{\mathrm{f}}}{L_{\mathrm{range}}} \Delta E_{\mathrm{s,max}} \leqslant E_{\mathrm{s}}(0) - E_{\mathrm{s}}(t_{\mathrm{f}}) \leqslant \frac{s_{\mathrm{f}}}{L_{\mathrm{range}}} \Delta E_{\mathrm{s,max}}, \tag{31}$$

where $\Delta E_{\mathrm{s,max}}$ is the maximum allowable energy change during the travel range, which can be calculated as

$$\Delta E_{\mathrm{s,max}} = \frac{x_{\mathrm{s}} n_{\mathrm{s}} C_{\mathrm{s}}}{2} \left(u_{\mathrm{s}}^2(\mathrm{soc}_{\mathrm{s,max}}) - u_{\mathrm{s}}^2(\mathrm{soc}_{\mathrm{s,min}}) \right). \tag{32}$$

The cost of the FC system includes the capital cost and the degradation cost. The degradation is converted into its equivalent capital cost according to the FC SoD. Then the FC cost is computed by

$$C_{\mathrm{fcs}} = \frac{(1 + \mathrm{sod}(t_{\mathrm{f}}))\, \beta_{\mathrm{fcs}} P_{\mathrm{fcb,max}} x_{\mathrm{fc}}}{L_{\mathrm{a}} y_{\mathrm{trk}}} \mathrm{CF}, \tag{33}$$

with β_{fcs} being the FC system price per kW and CF denoting the cost factor that is related to the truck service period and the yearly interest rate p_{y}. The cost factor is described as

$$\mathrm{CF} = 1 + p_{\mathrm{y}} \frac{y_{\mathrm{trk}} + 1}{2}, \tag{34}$$

and it also applies to the cost of energy buffer and electric machine. The cost of the energy buffer is calculated as

$$C_{\mathrm{eb}} = \frac{\beta_{\mathrm{eb}} x_{\mathrm{s}} n_{\mathrm{s}} C_{\mathrm{s}}}{2 L_a y_{\mathrm{trk}}} \left(u_{\mathrm{s,max}}^2 - u_{\mathrm{s,min}}^2 \right) \mathrm{CF}, \tag{35}$$

with β_{eb} being the energy buffer price per kWh, $u_{\mathrm{s,min}}$ and $u_{\mathrm{s,max}}$ denoting the minimal and maximal OCV of the cell. The cost of the electric machine is computed as

$$C_{\mathrm{em}} = \frac{\beta_{\mathrm{em}} x_{\mathrm{em}} P_{\mathrm{emb,max}}}{L_{\mathrm{a}} y_{\mathrm{trk}}} \mathrm{CF}, \tag{36}$$

where β_{em} is the electric machine price per kW and $P_{\mathrm{emb,max}} = \max_k (T_{\mathrm{emb,max,k}}\, \omega_k)$ represents the peak power of the baseline electric machine, where k is any feasible operating point.

B. Chance-Constrained Optimization

The wheel power demand in (1) directly translates to a minimum size of electric machine and cumulative power provided by the FC system and energy buffer. It is of interest to investigate smaller component sizes that provide requested power most of the time, except perhaps at a few instances. The idea is to get robust component sizes by removing outliers in noisy measurements (or unrealistic reference points), and also enabling a sensitivity analysis on how component sizes change with demanded power, while trying to maintain travel time requirements.

Thus, the constraint (1) can be rewritten as a chance-constraint,

$$\mathbb{P} \left(\begin{array}{c} \min \left(P_{\mathrm{st}}(t) \eta_{\mathrm{bb}}, \frac{P_{\mathrm{st}}(t)}{\eta_{\mathrm{bb}}} \right) + P_{\mathrm{fcs}}(t) \eta_{\mathrm{bo}} \\ \geqslant P_{\mathrm{wh}}(t) + P_{\mathrm{loss,em}}(t) + P_{\mathrm{aux}}(t) \end{array} \right) \geqslant \gamma, \tag{37}$$

where $\gamma \in (0, 1]$ is a pre-assigned probability for constraint satisfaction. Notice that the equality (1) has been relaxed to inequality, within the parentheses in (37), in order to ensure problem convexity. However, it has been shown in previous studies that for the optimal solution, the relaxation will indeed hold with equality, as otherwise energy will be wasted unnecessarily [47], [48]. Furthermore, the inequality outside the parentheses in (37) requires that the FC and the energy buffer are able to deliver what is demanded by the driving cycle, up to a given probability. Any $\gamma < 1$ in (37) allows downsizing the FC, energy buffer, electric machine and the power electronics by delivering less power than demanded for some time intervals, which consequently will cause the truck speed to deviate from that requested by the driving cycles. In this study we require delivering demanded speed as close as possible and traversing the cycle with as close travel time as possible, but still not delivering unnecessarily more power than what is needed to satisfy (37). Due to didactic reasons, we state this as a verbal constraint in the problem description below. Later, in Section IV, a detailed mathematical treatment is provided after the main idea of the proposed method is explained.

By summarizing the objective function and all constraints, the problem can be formulated as

$$\min_{x_{\mathrm{em}}, x_{\mathrm{fc}}, x_{\mathrm{s}}, P_{\mathrm{fcs}}, P_{\mathrm{s}}, T_{\mathrm{brk}}, E_{\mathrm{s}}, \mathrm{sod}} J, \tag{38a}$$

$$\text{s.t. } \mathbb{P} \left(\begin{array}{c} \min \left(P_{\mathrm{st}}(t) \eta_{\mathrm{bb}}, \frac{P_{\mathrm{st}}(t)}{\eta_{\mathrm{bb}}} \right) + P_{\mathrm{fcs}}(t) \eta_{\mathrm{bo}}, \\ \geqslant P_{\mathrm{wh}}(t) + P_{\mathrm{loss,em}}(t) + P_{\mathrm{aux}}(t) \end{array} \right) \geqslant \gamma, \tag{38b}$$

$$T_{\mathrm{em}}(t) = T_{\mathrm{dem}}(t) + T_{\mathrm{brk}}(t), \tag{38c}$$

$$T_{\mathrm{emb,min}}(\omega(t)) x_{\mathrm{em}} \leqslant T_{\mathrm{em}}(t) \leqslant T_{\mathrm{emb,max}}(\omega(t)) x_{\mathrm{em}}, \tag{38d}$$

$$0 \leqslant P_{\mathrm{fcs}}(t) \leqslant x_{\mathrm{fc}} P_{\mathrm{fcb,max}}, \tag{38e}$$

$$x_{\mathrm{fc,min}} \leqslant x_{\mathrm{fc}} \leqslant x_{\mathrm{fc,max}}, \tag{38f}$$

$$x_{\mathrm{fc}} R_{\mathrm{fcb,min}} \leqslant \dot{P}_{\mathrm{fcs}}(t) \leqslant x_{\mathrm{fc}} R_{\mathrm{fcb,max}}, \tag{38g}$$

$$\dot{\mathrm{sod}}(t) = d_0 \left(\frac{P_{\mathrm{fcs}}(t)}{x_{\mathrm{fc}}} \right)^2 + d_1 \frac{P_{\mathrm{fcs}}(t)}{x_{\mathrm{fc}}} + d_2, \tag{38h}$$

$$\mathrm{sod}(0) = 0, \tag{38i}$$

$$\mathrm{sod}(t_{\mathrm{f}}) \leqslant \Delta \mathrm{sod}, \tag{38j}$$

$$\dot{E}_{\mathrm{s}} = -P_{\mathrm{s}}(t), \tag{38k}$$

$$\frac{x_{\mathrm{s}} n_{\mathrm{s}} C_{\mathrm{s}}}{2} \left(u_{\mathrm{s}}^2(\mathrm{soc}_{\mathrm{s,min}}) - u_{0\mathrm{s}}^2 \right) \leqslant E_{\mathrm{s}}(t), \tag{38l}$$

$$\frac{x_{\rm s} n_{\rm s} C_{\rm s}}{2}\left(u_s^2(\mathrm{soc}_{\rm s,max}) - u_{0\rm s}^2\right) \geqslant E_{\rm s}(t), \tag{38m}$$

$$-\frac{s_{\rm f}}{L_{\rm range}}\Delta E_{\rm s,max} \leqslant E_{\rm s}(0) - E_{\rm s}(t_{\rm f}) \leqslant \frac{s_{\rm f}}{L_{\rm range}}\Delta E_{\rm s,max}, \tag{38n}$$

$$i_{\rm s,min}\sqrt{x_{\rm s} n_{\rm s}\left(\frac{2E_{\rm s}(t)}{C_{\rm s}} + x_{\rm s} n_{\rm s} u_{0\rm s}^2\right)} \leqslant P_{\rm s}(t), \tag{38o}$$

$$i_{\rm s,max}\sqrt{x_{\rm s} n_{\rm s}\left(\frac{2E_{\rm s}(t)}{C_{\rm s}} + x_{\rm s} n_{\rm s} u_{0\rm s}^2\right)} \geqslant P_{\rm s}(t), \tag{38p}$$

$$\int_0^{t_{\rm f}} |P_{\rm s}(t)|\,\mathrm{d}t \leqslant \frac{2N_{\rm cl} x_{\rm s} n_{\rm s} E_{\rm cl} s_{\rm f}}{y_{\rm trk} L_{\rm a}}, \tag{38q}$$

$$x_{\rm s,min} \leqslant x_{\rm s} \leqslant x_{\rm s,max}, \tag{38r}$$

drive as close as possible to demanded speed and travel time. (38s)

The optimization variables consist of the scalar scaling variables $x_{\rm em}$, $x_{\rm fc}$, $x_{\rm s}$, the time dependent control variables $P_{\rm fcs}$, $P_{\rm s}$ and $T_{\rm brk}$, and the time dependent state variables $E_{\rm s}$ and sod. The problem has, in fact, two additional state variables that are not written in a standard form. The constraint (38g) limits the baseline FC power variation rate to be within $[R_{\rm fcb,min}, R_{\rm fcb,max}]$, which means that $P_{\rm fcs}$ can be regarded as a state in the problem. Similarly, the constraint on the cycle life (38q) can be written without the integral form, by introducing an additional state with the time derivative equal to the absolute value of the energy buffer power.

The objective function is convex with respect to $P_{\rm fcs}$, $E_{\rm s}$, $x_{\rm fc}$, $x_{\rm s}$ and $x_{\rm em}$. The convexity of the chance-constraint (38b) for power balance and the verbal constraint (38s) will be discussed in Section IV. The constraints (38c)–(38g), (38i)–(38n), (38r) are affine relations, and therefore convex. The constraints (38o)-(38q) are nonlinear, but they define a convex set. The former two can be recognized as a geometric mean function, which is concave in $x_{\rm s}$ and $E_{\rm s}$, while the latter is an absolute value, which is convex in $P_{\rm s}$. The constraint (38h) is a nonlinear equality constraint and thus is not convex.

It can be concluded that in the present form, problem (38) is a nonlinear and non-convex dynamic program that includes both time dependent and scalar optimization variables. Moreover, the problem includes a chance constraint and related constraints in (38s) that are yet to be defined. As the problem is difficult to solve, we propose first decomposing it into two sub-problems. Then, remodelling steps are performed to convexify both sub-problems.

IV. Optimization Method

In this section, we show that problem (38) can be translated to an equivalent deterministic problem, decomposed into two sub-problems. Then, we show convex modelling steps such that the problem can be solved by sequential convex programming.

TABLE II
Truck Specifications and Environment Parameters

Parameter (unit)	Value
Max. gross weight, $m_{\rm trk}$ (ton)	18 /27 /33 /40
Front area, $A_{\rm f}$ (m^2)	10
Final gear ratio, $k_{\rm gr}$ (-)	3
Wheel radius, $r_{\rm wh}$ (m)	0.5
[a]Wheel inertia, $J_{\rm wh}$ (kgm^2)	90
Baseline electric machine inertia, $J_{\rm em}$ (kgm^2)	1.92
Auxiliary power, $P_{\rm aux}$ (kW)	5.6
Gravitational acceleration, g ($\mathrm{m/s}^2$)	9.81
Air density, $\rho_{\rm a}$ ($\mathrm{kg/m}^3$)	1.184
Rolling resistance coefficient, $C_{\rm r}$ (-)	0.007
Aerodynamic drag coefficient, $C_{\rm d}$ (-)	0.7

[a] Estimated according to 4×2 axle configuration.

A. Deterministic Programming

It is possible to translate the chance-constrained optimization problem (38) into a deterministic program. The constraint satisfaction with a selected probability $\gamma \in (0, 1]$ can be seen as finding an upper bound, $P_{\rm wh}^{\max}(\gamma)$, on the wheel power demand to make (39) hold, i.e.

$$P_{\rm wh}^{\max}(\gamma) = \max\left(P_{\rm wh}(t) \in \mathcal{P}_{\rm wh} : \mathrm{cdf}(P_{\rm wh}(t)) \leqslant \gamma\right). \tag{39}$$

Here,

$$\mathrm{cdf}(P_{\rm wh}(t)) = \mathbb{P}\left(P_{\rm wh}(t) \in \mathcal{P}_{\rm wh} : P_{\rm wh}(t) \leqslant P_{\rm wh}^{\max}(1)\right) \tag{40}$$

defines the CDF of the wheel power demand $P_{\rm wh}(t)$, with

$$\mathcal{P}_{\rm wh} = \left\{P_{\rm wh}(t)\right\}, \quad \forall t \in [0, t_{\rm f}],$$
$$P_{\rm wh}^{\max}(1) = \max\left(P_{\rm wh}(t) \in \mathcal{P}_{\rm wh}\right), \tag{41}$$

where $P_{\rm wh}^{\max}(1)$ is the upper limit of constraint satisfaction with a probability $\gamma = 1$.

For the given driving cycles, the wheel power demand can be calculated from longitudinal vehicle dynamics, noting that the truck mass significantly differs with its vocation. We assume that the maximum gross weight of trucks for applications of urban delivery, regional delivery, construction and long-haul is 18, 27, 33, and 40 tons, respectively [20], [49]. The truck specifications and environmental parameters are listed in Table II. According to ACEA driving cycles, the maximum demanded acceleration is $2\,\mathrm{m/s}^2$, which might not be reasonable for all trucks. The excessive acceleration can result in unrealistic power requirements. For example, the peak wheel power demand is estimated to reach $1.30\,\mathrm{MW}$, $1.61\,\mathrm{MW}$, $1.84\,\mathrm{MW}$, and $2.44\,\mathrm{MW}$ in applications of urban delivery, regional delivery, construction, and long-haul trucking.

The cumulative distribution function of the estimated power demand for the four trucking applications is shown in Fig. 7. It can be seen that high peak power demands happen rarely. For instance, the probability is only 4% when the power demand exceeds $319\,\mathrm{kW}$ for urban delivery, $275\,\mathrm{kW}$ for regional delivery, $370\,\mathrm{kW}$ for construction, and $339\,\mathrm{kW}$ for long-haul application. Therefore, a selected $\gamma \in (0, 1]$ makes it possible

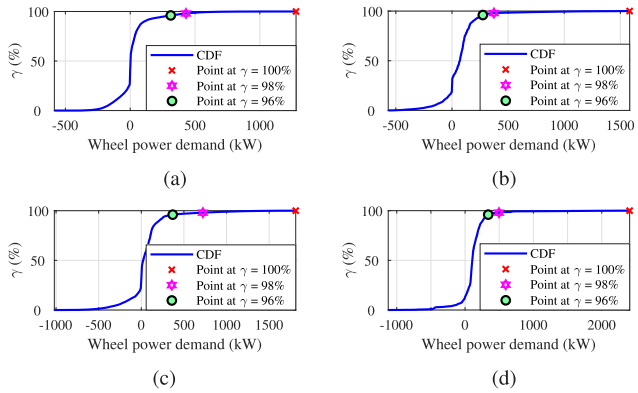

Fig. 7. Cumulative distribution function of the wheel power demand for different trucking applications. (a) Urban delivery. (b) Regional delivery. (c) Construction. (d) Long-haul.

TABLE III
UPPER BOUNDS OF WHEEL POWER DEMAND SATISFYING PROBABILITIES

Driving cycles	$P_{\mathrm{wh}}^{\max}(1)$ kW	$P_{\mathrm{wh}}^{\max}(0.98)$ kW	$P_{\mathrm{wh}}^{\max}(0.96)$ kW
Urban delivery	1296	438	319
Regional delivery	1605	375	275
Construction	1837	735	370
Long-haul	2444	496	339

to use a lower power rating of the electric machine, the FC, the energy buffer and the associated power electronic converters, leading to a lower cost. Example points when γ equals to 96%, 98%, and 100% are marked in Fig. 7, while the upper bounds of the corresponded delivered power satisfying these probabilities are listed in Table III. Clearly, the selection of γ also determines driveability, as bigger γ allows more aggressive driving.

The upper bound of the wheel power demand, $P_{\mathrm{wh}}^{\max}(\gamma)$, can be obtained from Fig. 7 once the value of γ is determined. Then, the power balance in constraint (38b) can be written as a deterministic constraint

$$\min\left(P_{\mathrm{st}}(t)\eta_{\mathrm{bb}}, \frac{P_{\mathrm{st}}(t)}{\eta_{\mathrm{bb}}}\right) + P_{\mathrm{fcs}}(t)\eta_{\mathrm{bo}} - P_{\mathrm{loss,em}}(t) - P_{\mathrm{aux}}(t) \geqslant \min(P_{\mathrm{wh}}(t), P_{\mathrm{wh}}^{\max}(\gamma)), \quad (42)$$

for all time instances, which means that the delivered power series is saturated with $P_{\mathrm{wh}}^{\max}(\gamma)$ during the truck movement.

Therefore, the stochastic program (38) is then translated to a deterministic program with the chance-constraint (38b) replaced by the deterministic constraint (42).

B. Problem Decomposition

Since the power rating of the electric machine is only determined by the CDF of the wheel power demand for a given driving cycle, the electric machine sizing can be performed offline. Once the electric machine is sized, the velocity trajectory of trucks can be obtained with respect to the verbal constraint (38s). The remaining component sizing and energy management can be dealt with using the determined electric machine size and the obtained velocity trajectory.

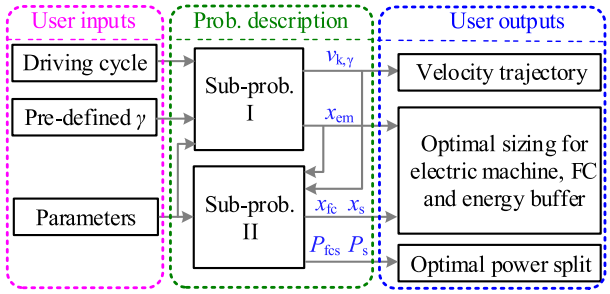

Fig. 8. Problem decomposition and optimization framework.

Therefore, the solution to the deterministic program derived from the stochastic program (38) can be decomposed by solving two sub-problems sequentially, as shown in Fig. 8. The aim of each sub-problem can be summarized as

- Sub-problem I: find a proper sizing of the electric machine and filter out the velocity trajectory corresponding to the wheel power demand $P_{\mathrm{wh},\gamma}(t)$ with the aim to drive as close as possible to the demanded speed and travel time but with the delivered wheel power following a cumulative probability γ;
- Sub-problem II: find an optimal sizing for FC and energy buffer as well as the optimal power split between each power source to minimize the summation of the components cost and the operational cost by using the electric machine sizing and velocity trajectory obtained from Sub-problem I.

We assume that the equivalent mass of all rotational parts does not change significantly with the electric machine sizing in Sub-problem I.

After solving Sub-problem I, the delivered power trajectory, denoted as $P_{\mathrm{wh},\gamma}(t)$, is possible to obtain from the new velocity trajectory. This is enforced by

$$\min\left(P_{\mathrm{st}}(t)\eta_{\mathrm{bb}}, \frac{P_{\mathrm{st}}(t)}{\eta_{\mathrm{bb}}}\right) + P_{\mathrm{fcs}}(t)\eta_{\mathrm{bo}} - P_{\mathrm{loss,em}}(t) - P_{\mathrm{aux}}(t) \geqslant P_{\mathrm{wh},\gamma}(t). \quad (43)$$

With $P_{\mathrm{wh}}^{\max}(\gamma)$ determined, constraint (42) can be replaced by constraint (43) after solving Sub-problem I, which is used as the power balance constraint in Sub-problem II. The reason for this is that (43) is more restrictive, i.e.

$$P_{\mathrm{wh},\gamma}(t) \geqslant \min(P_{\mathrm{wh}}(t), P_{\mathrm{wh}}^{\max}(\gamma)), \forall t \in [0, t_{\mathrm{f}}]. \quad (44)$$

C. Sub-Problem for Limiting Demanded Power and Electric Machine Sizing

Since Sub-problem I can be separated from problem (38), the sampling in distance is performed to simplify the introduction of constraints on the travel time. Let the following sets define driving and stand-still instances

$$\mathcal{S}_{\mathrm{drv}} = \{s \in [0, s_{\mathrm{f}}] \mid E_{\mathrm{k}}(s) > 0\}, \quad (45)$$

$$\mathcal{S}_{\mathrm{ss}} = \{s \in [0, s_{\mathrm{f}}] \mid E_{\mathrm{k}}(s) = 0\}, \quad (46)$$

where s is the distance instance. The kinetic energy of the truck in the distance-domain, when $\gamma = 1$ is assumed, can be computed

by

$$E_{\mathrm{k}}(s) = \frac{1}{2}(m_{\mathrm{trk}} + m_{\mathrm{r}})v(s)^2, \tag{47}$$

with $v(s)$ being the distance-based speed from the original driving cycle. Once $P_{\mathrm{wh}}^{\max}(\gamma)$ is obtained, the maximum power of the electric machine can be determined with the scaling factor calculated as

$$x_{\mathrm{em}} = \frac{P_{\mathrm{wh}}^{\max}(\gamma)}{P_{\mathrm{emb,max}}}. \tag{48}$$

The problem of closely following the original speed, while keeping the delivered power limited and trying to finish the route in about the same time, can be formulated as

$$\min_{\sigma, E_{\mathrm{k},\gamma}, F_{\mathrm{wh},\gamma}, t_\gamma} c_{\mathrm{time}}\sigma + \int_0^{s_{\mathrm{f}}} \left(E_{\mathrm{k},\gamma}(s) - E_{\mathrm{k}}(s)\right)^2 \mathrm{d}s, \tag{49a}$$

$$\frac{\mathrm{d}E_{\mathrm{k},\gamma}(s)}{\mathrm{d}s} = -\frac{\rho_a C_d A_f}{m_{\mathrm{trk}} + m_r} E_{\mathrm{k},\gamma}(s) + F_{\mathrm{wh},\gamma}(s) - F_\alpha(s), \tag{49b}$$

$$\frac{\mathrm{d}t_\gamma(s)}{\mathrm{d}s} = \begin{cases} \frac{1}{\sqrt{2E_{\mathrm{k},\gamma}(s)/(m_{\mathrm{trk}}+m_r)}}, & \forall s \in \mathcal{S}_{\mathrm{drv}} \\ \Delta t_{\mathrm{ss}}(s)\delta(s), & \forall s \in \mathcal{S}_{\mathrm{ss}} \end{cases}, \tag{49c}$$

$$0 < E_{\mathrm{k},\gamma}(s) \leqslant \max_{\mathrm{s}}(E_{\mathrm{k}}(s)), \quad \forall s \in \mathcal{S}_{\mathrm{drv}}, \tag{49d}$$

$$E_{\mathrm{k},\gamma}(s) = 0, \quad \forall s \in \mathcal{S}_{\mathrm{ss}}, \tag{49e}$$

$$t_\gamma(0) = 0, \quad t_\gamma(s_{\mathrm{f}}) \leqslant t(s_{\mathrm{f}}) + \sigma, \tag{49f}$$

$$F_{\mathrm{wh},\gamma}(s) \geqslant -\frac{P_{\mathrm{wh}}^{\max}(\gamma)}{\sqrt{2E_{\mathrm{k},\gamma}(s)/(m_{\mathrm{trk}} + m_{\mathrm{r}})}}, \forall s \in \mathcal{S}_{\mathrm{drv}}, \tag{49g}$$

$$F_{\mathrm{wh},\gamma}(s) \leqslant \frac{P_{\mathrm{wh}}^{\max}(\gamma)}{\sqrt{2E_{\mathrm{k},\gamma}(s)/(m_{\mathrm{trk}} + m_{\mathrm{r}})}}, \forall s \in \mathcal{S}_{\mathrm{drv}}, \tag{49h}$$

$$\frac{T_{\mathrm{emb,min}}(s) x_{\mathrm{em}} k_{\mathrm{gr}}}{r_{\mathrm{wh}}} \leqslant F_{\mathrm{wh},\gamma}(s) \leqslant \frac{T_{\mathrm{emb,max}}(s) x_{\mathrm{em}} k_{\mathrm{gr}}}{r_{\mathrm{wh}}}, \forall s, \tag{49i}$$

where the objective function in (49a) is trying to deliver similar speed and travel time as the original driving cycle. In practice, this means that the acceleration is limited for some instances due to the limited power rating of the electric machine while higher speed is allowed for some other instances to make sure that the truck still arrives on time. When γ is too low it may not be possible to maintain the desired travel time and, hence, the constraint on final time is modeled as a soft constraint, where σ is a slack variable and c_{time} is a weighting coefficient penalizing longer time. The variable $E_{\mathrm{k},\gamma}(s)$ denotes the truck kinetic energy when the delivered power has a cumulative probability not greater than γ. The constraint (49b) represents the dynamics of the kinetic energy and can be derived from (2) with $F_\alpha(s)$ being the summation of all forces related to the road slope. The constraint (49c) describes the time dynamics where the time difference is computed by integration of the inverse speed over the traveled distance when the truck is moving; when the truck is standing still, a Dirac function, $\delta(s)$, is used to account for the standstill time, Δt_{ss}. The constraint (49d) ensures $E_{\mathrm{k},\gamma}(s)$ to be greater than 0 but smaller than the maximum original kinetic energy. The constraint (49e) keeps the truck having zero kinetic energy at stand-still instances. The constraint (49f) enforces the initial time to 0 and includes the soft constraint on the final time to ensure the truck driver arrives at the destination in a similar time as that of the original driving cycle. The constraints (49g) and (49h) limit the wheel force with the upper bound of the wheel power demand $P_{\mathrm{wh}}^{\max}(\gamma)$. The constraint (49i) is the wheel force limit computed from the torque bound of the electric machine. In principle, only upper bound of the wheel force is required for a given γ, but here the lower bound is also applied to limit the regenerative braking torque, which does not affect the component sizing [50], [51].

The optimization variables include the scalar scaling variable σ, distance dependent control variable $F_{\mathrm{wh},\gamma}$, and state variables $E_{\mathrm{k},\gamma}$ and t_γ. As can be seen, the objective function is convex with respect to σ and $E_{\mathrm{k},\gamma}$. The constraints (49b), (49d)–(49f) are affine relations, and thus convex. The constraints (49c), (49g) and (49h) are nonlinear and (49i) also contains the same nonlinear term that describes the torque limit at the constant power region of the electric machine. Therefore, both of them are not convex.

To preserve the convexity, the constraint (49c) can be relaxed as an inequality,

$$\frac{\mathrm{d}t_\gamma(s)}{\mathrm{d}s} \geqslant \begin{cases} \frac{1}{\sqrt{2E_{\mathrm{k},\gamma}(s)/(m_{\mathrm{trk}}+m_r)}} & \forall s \in \mathcal{S}_{\mathrm{drv}} \\ \Delta t_{\mathrm{ss}}(s)\delta(s) & \forall s \in \mathcal{S}_{\mathrm{ss}} \end{cases}, \tag{50}$$

thus becoming a convex constraint. It has been shown in a similar problem [52] that the constraint is tight at the optimal solution and the solution to the relaxed problem is identical to the solution of the original problem. The nonlinear term in the constraints (49g)–(49i), $\frac{P_{\mathrm{wh}}^{\max}(\gamma)}{\sqrt{E_{\mathrm{k},\gamma}(s)/(m_{\mathrm{trk}} + m_{\mathrm{r}})}}$, can be linearized by a first-order Taylor expansion at the kinetic energy when $\gamma = 1$, shown as

$$\frac{P_{\mathrm{wh}}^{\max}(\gamma)}{\sqrt{nE_{\mathrm{k},\gamma}(s)}} = \frac{P_{\mathrm{wh}}^{\max}(\gamma)}{\sqrt{nE_{\mathrm{k}}(s)}} - \frac{P_{\mathrm{wh}}^{\max}(\gamma)}{2\sqrt{nE_{\mathrm{k}}(s)^3}} \left(E_{\mathrm{k},\gamma}(s) - E_{\mathrm{k}}(s)\right), \tag{51}$$

with $n = 2/(m_{\mathrm{trk}} + m_{\mathrm{r}})$. Therefore, (51) shows affine relation and constraints (49g)–(49i) are converted into convex constraints. To reduce the linearization error, sequential convex programming is performed by iteratively updating E_{k} with the latest $E_{\mathrm{k},\gamma}$ after solving problem (49) until the solution stops changing. The iterative procedure for minimizing linearization error is illustrated in Fig. 9.

D. Sub-Problem for Power Sources Sizing and Energy Management

After performing the electric machine sizing in Sub-problem I, the cost of the electric machine can be excluded from the objective function in problem (38). Sub-problem II can then be written as

$$\min(C_{\mathrm{H2}} + C_{\mathrm{ele}} + C_{\mathrm{fcs}} + C_{\mathrm{eb}}), \tag{52}$$

subject to (38c)–(38r) and (43).

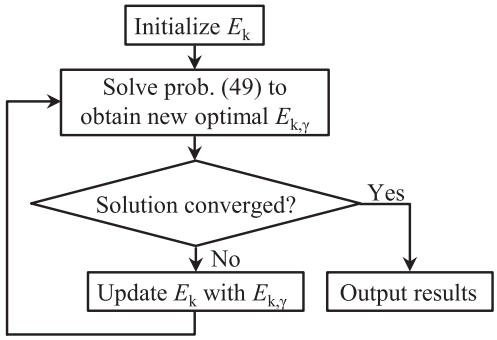

Fig. 9. Iterative procedure for solving Sub-problem I to minimize linearization error.

The FC and the energy buffer are designed to prioritize the delivery of propulsion power while the excessive braking power can be handled by mechanical braking. The amount of mechanical braking torque is affected by the capacity of the energy buffer. To avoid the calculation of mechanical braking torque in the optimization [53], the equality constraint in (38c) can be relaxed as an inequality constraint, which can be expressed as

$$T_{\rm em}(t)\geqslant T_{\rm dem}(t), \tag{53}$$

and the optimization variable $T_{\rm brk}$ can be dropped out.

To convexity the constraint (38h), a variable change sodx is introduced, which is also used to scale up the SoD variation over one driving cycle to improve the solver convergence. The term sodx can then be written as

$$\mathrm{sodx}(t)=\frac{\mathrm{sod}(t)}{\Delta\mathrm{sod}}x_{\rm fc}, \tag{54}$$

where $\mathrm{sod}(t)\in[0,\Delta\mathrm{sod}]$ with $t\in[0,t_{\rm f}]$. At the beginning of the driving cycle $\mathrm{sodx}(0)=0$ and at the end of the driving cycle, $\mathrm{sodx}(t_{\rm f})\leqslant x_{\rm fc}$. Take the derivative of (54) to obtain

$$\dot{\mathrm{sodx}}(t)=\dot{\mathrm{sod}}(t)\frac{x_{\rm fc}}{\Delta\mathrm{sod}}. \tag{55}$$

Therefore, constraint (38h), in a relaxed form, can be rewritten as

$$\dot{\mathrm{sodx}}(t)\geqslant\frac{1}{\Delta\mathrm{sod}}\left(d_0\frac{P_{\rm fcs}(t)^2}{x_{\rm fc}}+d_1P_{\rm fcs}(t)+d_2x_{\rm fc}\right), \tag{56}$$

which becomes a convex constraint [54].

To avoid the absolute value in constraint (38q), one more variable $P_{\rm sx}$ is introduced and (38q) can be relaxed as

$$\int_0^{t_{\rm f}}P_{\rm sx}(t){\rm d}t\leqslant\frac{2N_{\rm cl}x_sn_sE_{\rm cl}s_{\rm f}}{y_{\rm trk}L_{\rm a}}, \tag{57a}$$

$$P_{\rm sx}\geqslant P_s, \tag{57b}$$

$$P_{\rm sx}\geqslant -P_s. \tag{57c}$$

TABLE IV
MAIN PARAMETERS FOR CASE STUDY

Parameter (unit)	Value
[a]Hydrogen price, $\beta_{\rm h}$ (€/kg)	3.94
Hydrogen lower heating value, $C_{\rm h}$ (J/kg)	120×10^6
[b]Electricity unit price, $\beta_{\rm ele}$ (€/kWh)	0.12
[c]Fuel cell system price, $\beta_{\rm fcs}$ (€/kW)	77
[d]Energy buffer price, $\beta_{\rm eb}$ (€/kWh)	3880 for SC 1939 for LiC 243 for LiB
Travel range with one-time refueling, $L_{\rm range}$ (km)	600/ 600/ 600/ 800
Yearly average travel distance, $L_{\rm a}$ (km/year)	80 000
Truck average service year, $y_{\rm trk}$ (year)	10
Yearly interest rate, $p_{\rm y}$ (-)	5%
Efficiency of DC/DC converters, $\eta_{\rm bo}$ & $\eta_{\rm bb}$ (-)	0.98

[a] Adopted from [55] for renewable hydrogen.
[b] Adopted from world average price for household users in over 100 countries, which are calculated using the average annual household electricity consumption per year.
[c] Estimated according to the data based on 100,000 systems/year presented at the Annual Merit Review and Peer Evaluation Meeting in 2019.
[d] Provided by the vendors.

Since constraint (43) contains a $\min$ function, it can be reformulated as

$$\begin{aligned}&P_{\rm st}(t)\eta_{\rm bb}+P_{\rm fcs}(t)\eta_{\rm bo}-P_{\rm loss,em}(t)-P_{\rm aux}(t)\geqslant P_{\rm wh,\gamma}(t),\\&\frac{P_{\rm st}(t)}{\eta_{\rm bb}}+P_{\rm fcs}(t)\eta_{\rm bo}-P_{\rm loss,em}(t)-P_{\rm aux}(t)\geqslant P_{\rm wh,\gamma}(t).\end{aligned} \tag{58}$$

We can see that Sub-problem II is convex and can be effectively solved by convex programming.

V. CASE STUDY

All simulations are conducted with CVX toolbox using solver MOSEK in MATLAB R2020b on a PC with the configuration of Intel Core i7-7700 K CPU 4.2 GHz and 64 GB RAM. The main parameters used for the case study are listed in Table IV.

A. Electric Machine Sizing and Modification of Velocity Trajectory

In this section, the electric machine sizing and the modification of the velocity trajectory for each driving cycle are analyzed and discussed.

1) Electric Machine Sizing: The maximum power of the electric machine is designed to satisfy a CDF of the upper bound of the wheel power demand. Fig. 7 shows that the upper bound of the wheel power demand monotonically decreases with the decrease of CDF. This means that a lower CDF value gives a lower upper bound of the wheel power demand, leading to a lower power rating of the electric machine and a lower cost accordingly. However, the power rating of the electric machine significantly influences the acceleration characteristic. The minimum upper bound of wheel power required for trucks specified in Table II with acceleration from 0 to 50 km/h within 25 s is computed to be 170 kW, 247 kW, 330 kW, and 360 kW for applications of urban delivery, regional delivery, construction, and long-haul, respectively. To satisfy this acceleration characteristic, the electric machine should have a corresponded rated power that covers 92.8 %, 94.3 %, 95.3 %, and 96.5 % of each

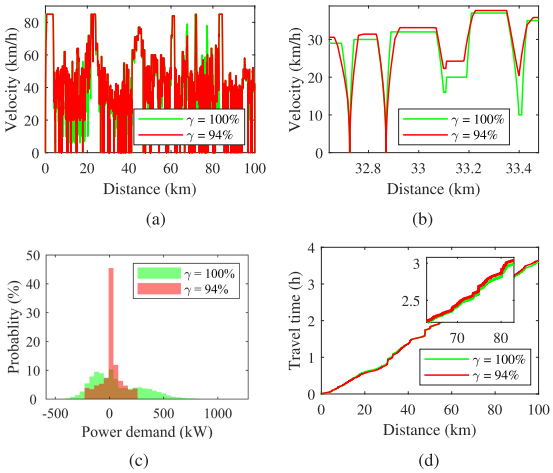

Fig. 10. Optimal results in the application of urban delivery. (a) Velocity trajectory. (b) Enlarged view of velocity. (c) Distribution of delivered power. (d) Travel time.

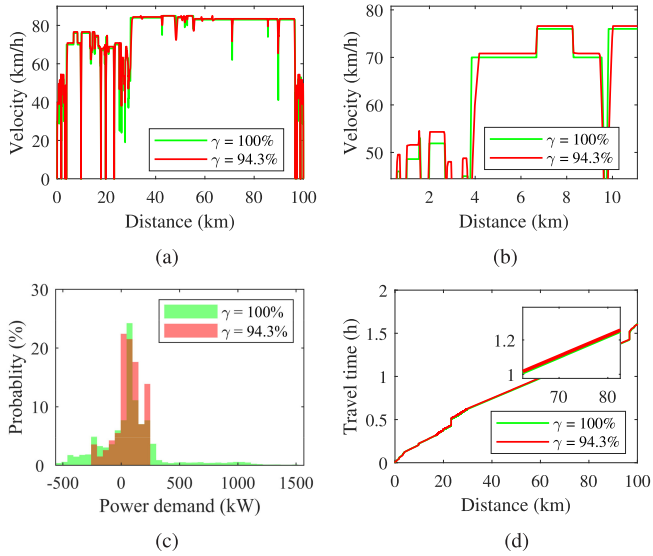

Fig. 11. Optimal results in the application of regional delivery.(a) Velocity trajectory. (b) Enlarged view of velocity. (c) Distribution of delivered power. (d) Travel time.

driving cycle power demand. In the case study, we select electric machines to meet the above acceleration characteristics and also to be able to cover at least 94 % of the wheel power demand in each driving cycle application. Therefore, the rated power of the electric machine is set as 218 kW, 247 kW, 330 kW, and 360 kW for applications of urban delivery, regional delivery, construction, and long-haul, respectively. The scaling factors are computed to be 1.09, 1.235, 1.65, and 1.8, respectfully.

2) Modification of Velocity Trajectory: With the maximum power of the electric machine determined, the velocity trajectory and the travel time for trucks in applications of urban delivery, regional delivery, construction, and long-haul can be obtained by solving problem (49). The problem is efficiently solved within 230 s for 6 iterations under the CVX environment. The optimal results at the selected γ for each driving cycle are compared with the original driving cycle for $\gamma = 1$ in Figs. 10, 11, 12, and 13. In the application of urban delivery, the velocity trajectory at $\gamma = 94\%$ almost exactly follows the original velocity of the driving cycle, see Fig. 10(a). The same trends can also be found in applications of regional delivery, construction, and long-haul. From the enlarged view of the velocity trajectory as shown in sub-figure (b) in Figs. 10, 11, 12, and 13, it can be seen that the velocity derivatives are reduced for the selected γ, due to the saturated delivered power, see sub-figures (c). We can also see that the velocity at some instances is higher than that at $\gamma = 100\%$. This is due to the time penalty in the objective function that ensures that the truck finishes the journey without much delay, even though the delivered peak wheel power is limited. Figs. 10, 11, 12, and 13(d) show that travel times along each journey at the selected γ and $\gamma = 100\%$ have a good coherence. The trucks can finish all journeys at about the same time compared to cases when $\gamma = 100\%$.

B. Fuel Cell and Energy Buffer Sizing

In this section, we show the optimal sizing of FC and energy buffer for several trucking applications using the determined

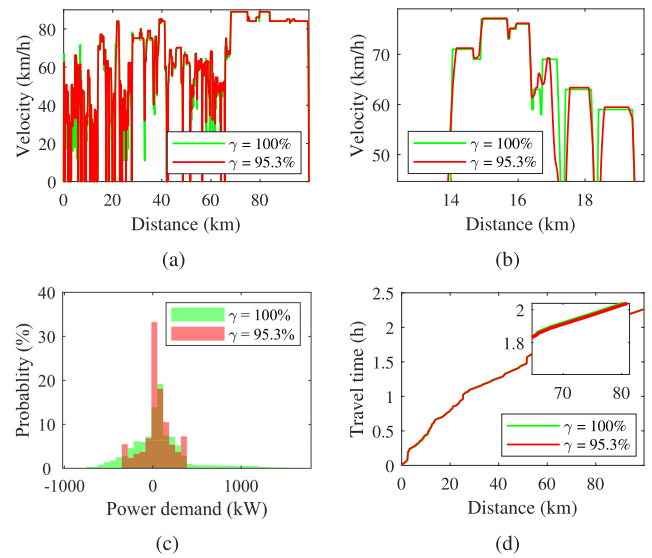

Fig. 12. Optimal results in the application of construction. (a) Velocity trajectory. (b) Enlarged view of velocity. (c) Distribution of delivered power. (d) Travel time.

electric machine and the modified velocity trajectories from Sub-problem I. Three different energy buffer technologies are also compared for each driving cycle.

The optimal sizing of power sources and their optimal power split are simultaneously obtained by solving Sub-problem II, which takes in average 130 s. The optimal values of the FC system and the energy buffer for the four driving cycles are shown in Table V. Since the total truck mass is assumed to be constant, the payload significantly differs with the change of the scaling parameters of FC and energy buffer. Therefore, a heavier FC and energy buffer will result in a less payload. This

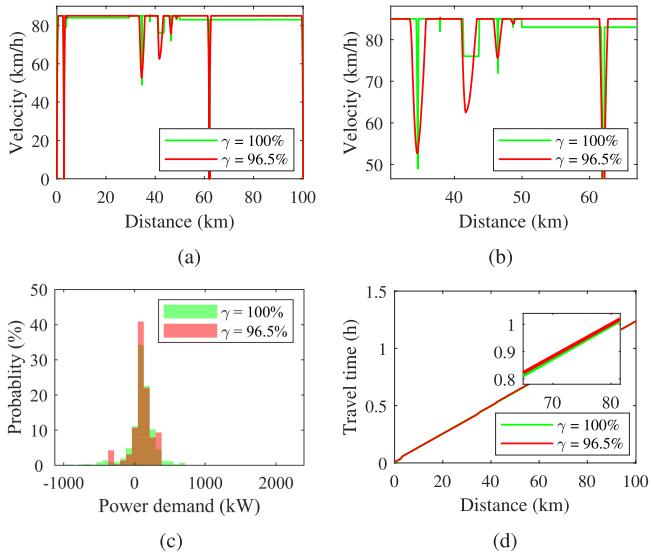

Fig. 13. Optimal results in the application of long-haul. (a) Velocity trajectory. (b) Enlarged view of velocity. (c) Distribution of delivered power. (d) Travel time.

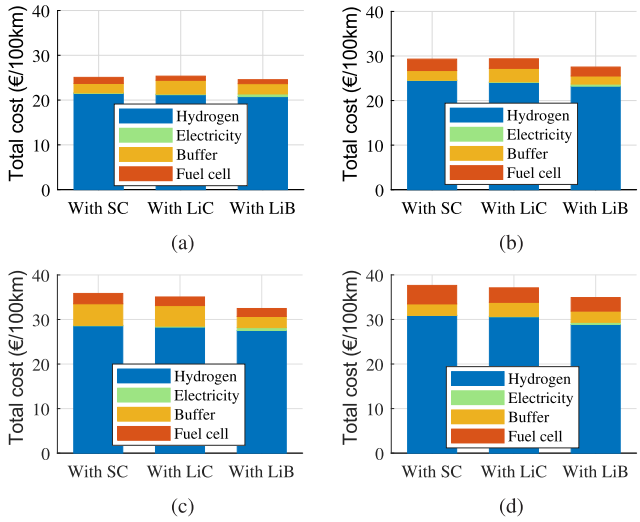

Fig. 14. Comparative total costs in the hybridization of different energy buffers among driving cycles. (a) Urban delivery. (b) Regional delivery. (c) Construction. (d) Long-haul.

TABLE V
OPTIMAL PARAMETERS OF FUEL CELL, ENERGY BUFFERS, CHASSIS MASS, AND TOTAL COST

Driving cycles	Buffers	$P_{\mathrm{fcs,max}}$	$P_{\mathrm{s,max}}$	$E_{\mathrm{s,max}}$	m_0	C_{total}
		kW	kW	kWh	kg	€/100km
Urban delivery	SC	111	652	3.43	16812	25.07
	LiC	76	223	9.93	17246	25.35
	LiB	73	478	59.51	16870	24.56
Regional delivery	SC	210	665	3.48	25375	29.30
	LiC	176	221	9.78	25822	29.37
	LiB	165	376	46.82	25642	27.52
Construction	SC	190	1496	7.82	30576	35.85
	LiC	158	336	14.92	31652	35.06
	LiB	147	512	64.71	31437	32.47
Long-haul	SC	340	791	4.14	37685	37.64
	LiC	266	226	10.15	38421	37.10
	LiB	248	517	64.98	38047	34.92

is reflected in the difference in m_0, which is also listed in Table V for comparison.

The FC maximum power in the case with an SC is much higher than that with LiC and LiB in all driving cycles, whereas the power rating of the FC is similar for all energy buffers with LiC and LiB. This is because SC has the lowest energy density and it cannot provide high power for a long time duration. By contrast, the LiC and LiB have a certain amount of energy capacity and they can provide relatively higher power resulting in relatively lower power ratings of FC. However, the energy capacity of the LiB in all driving cycles is much higher than that of the other energy buffers. For instance, the energy capacity of the LiB in urban delivery application is almost 6 times and 17 times than that of the LiC and the SC, respectively. Among all driving cycle applications, the truck using LiB shows the cheapest cost, which is around 2%, 6%, 9%, and 7% lower than that with SC as the energy buffer in urban delivery, regional delivery, construction, and long-haul application, respectively. However, the cost in the case of SC and LiC as the energy buffer does not seem to have big difference. In the driving cycles of urban delivery and regional delivery, the cost of the truck with the SC is slightly lower than that with LiC, but the trend is opposite for the construction and long-haul driving cycles. It is of interest to see that trucks with the LiC can accommodate more payload than others even though they show higher cost than trucks with LiB. The major reason for the difference in payloads is due to the different energy density of the three energy buffer technologies. As can be seen from Table I, the energy density of the LiB is 13.3 times and 3.3 times than that of the SC and the LiC. The difference of energy capacity also contributes to the difference in payloads. Taking the long-haul driving cycle as an example, the truck with LiC can carry 374 kg and 736 kg more payload than that with LiB and SC. The optimal design parameters with LiB in long-haul application are comparable with the parameters chosen in the XCIENT Fuel Cell truck.

To further understand the difference in total cost, cost distribution is presented in Fig. 14. The hydrogen cost accounts for the highest percentage, while the electricity cost is the lowest in each hybridization among all driving cycles. Also, the hydrogen cost in the hybridization with LiB shows the lowest expense compared to the hybridization with the SC and LiC among all driving cycles, due to a cheaper electricity unit price and high energy capacity of LiB. The FC cost in the case of LiB is the lowest compared to other energy buffers among all driving cycles, owing to the smallest FC power rating. The energy buffer cost differs for all driving cycles due to the big difference of the unit price and the energy capacity. For example, in the construction driving cycle, the energy capacity of the LiB and the LiC is around 8.27 times and twice that with the SC. However, the unit price of the SC is around 16 times and twice that of the LiB and the SC, respectively. For these reasons, the LiC cost is almost the same as the SC cost, whereas the LiB cost is around half of the SC cost. Due to the extremely cheap unit price of the LiB, its cost is still the lowest among all

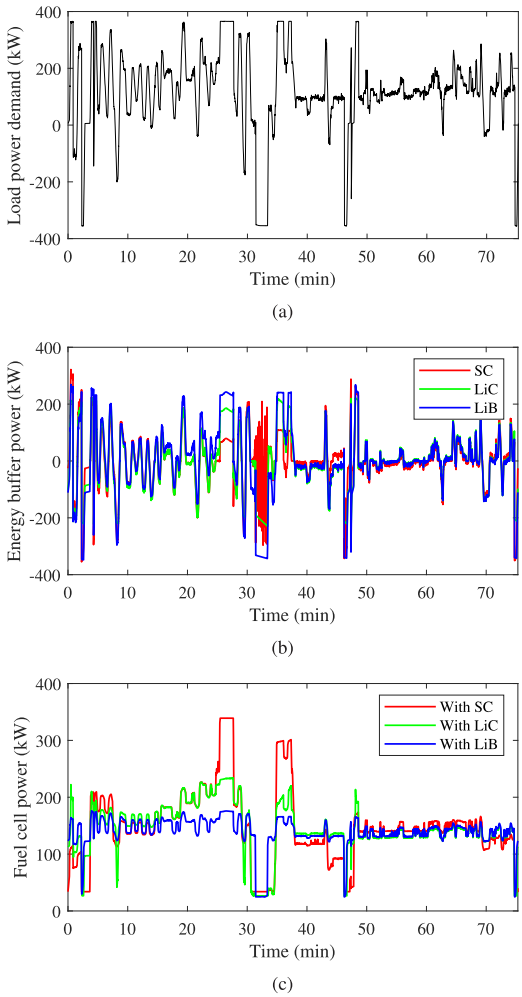

Fig. 15. Optimal power allocations in long-haul driving cycle. (a) Load power demand. (b) Energy buffer power. (c) Fuel cell power.

energy buffers for all driving cycles, despite its highest energy capacity.

C. Illustration of Power Allocation

Based on the optimal power rating of the FC and the energy capacity of the buffers, the optimal power allocations in long-haul driving cycle are illustrated as an example in Fig. 15. It is evident that the energy buffer mainly charges when the truck decelerates and discharges when the truck accelerates. Also, the power variation tendency of the energy buffer is severe and in general similar to the changes in demanded load power. By contrast, the FC power is relatively stable due to the FC power variation rate being limited within $\pm 10\%$ of the power rating per second. We can also see that in propulsion mode, the FC and energy buffer together provide the load demanded power. In the hybridization with the SC, the FC is forced to provide more power compared to that with the LiC and the LiB when the demanded power is continuously high. This is because the SC has limited energy capacity and cannot provide high power constantly, which can be seen in 25–28 min. Moreover, the FC power maintains a minimum output power, which is set as $10\,\%$ of its power rating in the case study. This enforces the energy buffer to be also charged by the FC power when working in regenerative braking mode. Among the investigated energy buffers, the LiB attempts to recuperate as much power as possible since it has relatively big energy capacity. The SC can only receive very small part of the negative power as shown in 30–34 min.

TABLE VI
REGENERATIVE BRAKING ENERGY

Driving cycles	Buffers	Generated energy	Recaptured energy	Percentage
		kWh	kWh	%
Urban delivery	SC	80.17	59.88	74.69
	LiC		59.67	74.43
	LiB		59.95	74.77
Regional delivery	SC	29.92	21.95	73.36
	LiC		22.35	74.72
	LiB		23.36	78.11
Construction	SC	76.24	58.40	76.61
	LiC		58.82	77.16
	LiB		59.36	77.87
Long-haul	SC	25.50	11.41	44.76
	LiC		14.12	55.38
	LiB		20.65	80.97

The recuperated braking energy of the different trucking appellations are compared in Table VI. In applications of urban delivery, regional delivery, and construction, the recaptured energy of the three energy buffers is similar and its percentages vary from $73\,\%$ to $78\,\%$. However, in long-haul application, the recaptured energy shows very big difference for the three energy buffers. As LiC has moderate energy capacity, the recaptured energy is slightly higher that that of the SC. The LiB shows moderate power capability and big energy capacity, which allows LiB to recuperate as much energy as possible.

VI. CONCLUSION

To investigate the cost-benefit of designing and operating FCHETs, we formulate a chance-constrained program. The component cost including the FC, the energy buffer, and the electric machine as well as the operational costs including hydrogen and electricity are considered when delivered power is satisfied in a probabilistic sense. The introduced chance-constrained nonlinear program is decomposed into two sub-problems and convex modeling steps are proposed to effectively solve them by sequential convex programming.

A case study is investigated showing that the maximum delivered power dramatically decreases as the satisfaction probability of the wheel power demand decreases. This allows downsizing the electric machine, FC, and energy buffer. Furthermore, it is shown that (1) the power rating of the electric machine is only around $18\,\%$ of the wheel peak power demand when the delivered power satisfying a given probability; (2) with the reduced power rating of the electric machine, trucks can finish the journey with a similar speed and in about the same time with that from the original driving cycle but without delivering unnecessarily high power; (3) using LiB as the energy buffer shows lowest total expense among all investigated energy buffer technologies, whereas using LiC as the energy buffer allows trucks to carry

more payload. For example, in long-haul application, the truck with LiC can carry 374 kg and 736 kg more payload than that with LiB and SC. (4) The proposed algorithm can be easily tailored to other types of hybrid EVs, including FC hybridized with SC and LiB simultaneously, and more details see [27].

A limitation of this study is that the proposed algorithm cannot be applied directly to general non-convex problems, which means that convex modeling steps are possibly required. Also, linear scaling is applied for the powertrain components, which may not be accurate when the optimal sizes are far from the baseline.

Future work related to this paper will be focused on several aspects. First, a more generic non-linear algorithm needs to be further developed for non-convex problems. Second, the selection of FC type for various vehicle applications can be conducted according to the specific requirement of each application. Third, the introduced method might be used to investigate a robust design optimization for FCHETs according to real-word truck operation. Forth, a moving horizon real-time energy management of FCHETs can be considered to improve the system efficiency and minimize the hydrogen consumption.

Appendix

A list of nomenclature is provided as a supplementary document.

Acknowledgments

The authors would also like to acknowledge Prof. Torbjörn Thiringer for the support and helpful discussions.

References

[1] "Reducting CO_2 emissions from heavy-duty vehicles." European Commission, Accessed: Jul. 15, 2021. [Online]. Available: https://ec.europa.eu/clima/policies/transport/vehicles/heavy_en

[2] L. Fan, Z. Tu, and S. H. Chan, "Recent development of hydrogen and fuel cell technologies: A review," *Energy Rep.*, vol. 7, pp. 8421–8446, 2021.

[3] T. Rudolf, T. Schurmannü, S. Schwab, and S. Hohmann, "Toward holistic energy management strategies for fuel cell hybrid electric vehicles in heavy-duty applications," *Proc. IEEE Proc. IRE*, vol. 109, no. 6, pp. 1094–1114, Jun. 2021.

[4] "Hyundai upgrades XCIENT fuel cell truck," *Fuel Cells Bull.*, vol. 2021, no. 6, p. 4, 2021.

[5] "Toyota unveils project portal 2.0 heavy truck," *Fuel Cells Bull.*, vol. 2018, no. 7, p. 1, 2018.

[6] "Hyundai delivers first XCIENT fuel cell trucks to Switzerland," *Fuel Cells Bull.*, vol. 2020, no. 8, p. 3, 2020.

[7] X. Wu, X. Hu, X. Yin, Y. Peng, and V. Pickert, "Convex programming improved online power management in a range extended fuel cell electric truck," *J. Power Sources*, vol. 476, 2020, Art. no. 228642.

[8] C. Geng, X. Jin, and X. Zhang, "Simulation research on a novel control strategy for fuel cell extended-range vehicles," *Int. J. Hydrogen Energy*, vol. 44, pp. 408–420, 2019.

[9] B. Vural *et al.*, "Fuel cell and ultra-capacitor hybridization: A prototype test bench based analysis of different energy management strategies for vehicular applications," *Int. J. Hydrogen Energy*, vol. 35, pp. 11161–11171, 2010.

[10] Y. Eren, O. Erdinc, H. Gorgun, M. Uzunoglu, and B. Vural, "A fuzzy logic based supervisory controller for an FC/UC hybrid vehicular power system," *Int. J. Hydrogen Energy*, vol. 34, pp. 8681–8694, 2009.

[11] M. Uzunoglu and M. S. Alam, "Modeling and analysis of an FC/UC hybrid vehicular power system using a novel-wavelet-based load sharing algorithm," *IEEE Trans. Energy Convers.*, vol. 23, no. 1, pp. 263–272, Mar. 2008.

[12] M. G. Garignano, R. Costa-Castelló, V. Roda, N. M. Nigro, S. Junco, and D. Feroldi, "Energy management strategy for fuel cell-supercapacitor hybrid vehicles based on prediction of energy demand," *J. Power Sources*, vol. 360, pp. 419–433, 2017.

[13] Y. Y. Q. Li, B. Su, J. Liu, and L. Ma, "Optimal energy management and control in multimode equivalent energy consumption of fuel cell/supercapacitor of hybrid electric tram," *IEEE Trans. Ind. Electron.*, vol. 66, no. 8, pp. 263–272, Aug. 2019.

[14] A. Ferrara, S. Jakubek, and C. Hametner, "Energy management of heavy-duty fuel cell vehicles in real-world driving scenarios: Robust design of strategies to maximize the hydrogen econoy and system lifetime," *Energy Convers. Manage.*, vol. 232, 2021, Art. no. 113795.

[15] B. Bendjedia, N. Rizoug, M. Boukhnifer, F. Bouchafaa, and M. Benbouzid, "Influence of secondary source technologies and energy management strategies on energy storage system sizing for fuel cell electric vehicles," *Int. J. Hydrogen Energy*, vol. 43, pp. 11614–11628, 2018.

[16] L. Xu, M. Ouyang, J. Li, F. Yang, L. Lu, and J. Hua, "Optimal sizing of plug-in fuel cell electric vehicles using models of vehicle performance and system cost," *Appl. Energy*, vol. 103, pp. 477–478, 2013.

[17] J. Marcinkoski, R. Vijayagoopal, J. Kast, and A. Duran, "Driving an industry: Medium and heavy duty fuel cell electric truck component sizing," *World Electric Veh. J.*, vol. 8, pp. 78–89, 2016.

[18] K. Sim, R. Vijayagopal, N. Kim, and A. Rousseau, "Optimization of component sizing for a fuel cell-powered truck to minimize ownership cost," *Energies*, vol. 12, pp. 1124–1136, 2019.

[19] A. Ravey, N. Watrin, B. Blunier, D. Bouquain, and A. Miraoui, "Energy-source-sizing methodology for hybrid fuel cell vehicles based on statistical description of driving cycles," *IEEE Trans. Veh. Technol.*, vol. 60, no. 9, pp. 4164–4174, Nov. 2011.

[20] M. Lu, G. Domingues-Olavarría, F. J. Márquez-Fernández, P. Fyhr, and M. Alaküla, "Electric drivetrain optimization for a commercial fleet with different degrees of electrical machine commonality," *Energies*, vol. 14, 2021, Art. no. 2989.

[21] Z. Song, H. Hofmann, J. Li, X. Han, X. Zhang, and M. Ouyang, "A comparison study of different semi-active hybrid energy storagesystem topologies for electric vehicles," *J. Power Sources*, vol. 274, pp. 400–411, 2015.

[22] Z. Hu *et al.*, "Multi-objective energy management optimization and parameter sizing for proton exchange membrane hybrid fuel cell vehicles," *Energy Convers. Manage.*, vol. 129, pp. 108–121, 2016.

[23] H. Jiang, L. Xu, J. Li, Z. Hu, and M. Ouyang, "Energy management and component sizing for a fuel cell/battery/supercapacitor hybrid powertrain based on two-dimensional optimization algorithms," *Energy*, vol. 177, pp. 386–396, 2019.

[24] L. Xu, C. D. Mueller, J. Li, M. Ouyang, and Z. Hu, "Multi-objective component sizing based on optimal energy management strategy of fuel cell electric vehicles," *Appl. Energy*, vol. 157, pp. 664–674, 2015.

[25] N. Murgovski, X. Hu, L. Johannesson, and B. Egardt, *Combined Design and Control Optimization of Hybrid Vehicles*. New York, NY, USA: Wiley, 2015.

[26] X. Hu, N. Murgovski, L. M. Johannesson, and B. Egardt, "Optimal dimensioning and power managementof a fuel cell/battery hybrid bus via convex programming," *IEEE/ASME Trans. Mechatronics*, vol. 20, no. 1, pp. 457–468, Feb. 2015.

[27] X. Hu, L. Johannesson, N. Murgovski, and B. Egardt, "Longevity-conscious dimensioning and power management of the hybrid energy storage system in a fuel cell hybrid electric bus," *Appl. Energy*, vol. 137, pp. 913–924, 2015.

[28] X. Wu, X. Hu, X. Yin, L. Li, Z. Zeng, and V. Pickert, "Convex programming energy management and components sizing of a plug-in fuel cell urban logistics vehicle," *J. Power Sources*, vol. 423, pp. 358–366, 2019.

[29] Y. Feng and Z. Dong, "Integrated design and control optimization of fuel cell hybrid mining truck with minimized lifecycle cost," *Appl. Energy*, vol. 270, 2020, Art. no. 115164.

[30] Q. Xun, Y. Liu, and E. Holmberg, "A comparative study of fuel cell electric vehicle hybridization with battery or supercapacitor," in *Proc. Int. Symp. Power Electron. Elect. Drives Automat. Emotion*, 2018, pp. 390–395.

[31] H. S. Das, C. W. Tan, and A. Yatim, "Fuel cell hybrid electric vehicles: A review on power conditioning units and topologies," *Renewable Sustain. Energy Rev.*, vol. 76, pp. 268–291, 2017.

[32] Q. Xun, S. Lundberg, and Y. Liu, "Design and experimental verification of a fuel cell/supercapacitor passive configuration for a light vehicle," *J. Energy Storage*, vol. 33, 2021, Art. no. 102110.

[33] X. Hu, N. Murgovski, L. Johannesson, and B. Egardt, "Energy efficiency analysis of a series plug-in hybrid electric bus with different energy management strategies and battery sizes," *Appl. Energy*, vol. 111, pp. 1001–1009, 2013.
[34] B. Egardt, N. Murgovski, M. Pourabdollah, and L. J. Mårdh, "Electromobility studies based on convex optimization: Design and control issues regarding vehicle electrification," *IEEE Control System Mag.*, vol. 34, no. 2, pp. 32–39, Apr. 2014.
[35] X. Hu, N. Murgovski, L. M. johannesson, and B. Egardt, "Comparison of three electrochemical energy buffers applied to a hybrid bus powertrain with simultaneous optimal sizing and energy management," *IEEE Trans. Intell. Transp. Syst.*, vol. 15, no. 3, pp. 1193–1205, Jun. 2014.
[36] P. Schneider, C. Sadeler, A.-C. Scherzer, N. Zamel, and D. Gerteisen, "Fast and reliable state-of-health model of a PEM cathode catalyst layer," *J. Electrochem. Soc.*, vol. 166, no. 4, pp. F322–F333, 2019.
[37] P. Ren, P. Pei, Y. Li, Z. Wu, D. Chen, and S. Huang, "Degradation mechanisms of proton exchange membrane fuel cell under typical automotive operating conditions," *Prog. Energy Combustion Sci.*, vol. 80, 2020, Art. no. 100859.
[38] Y. Yang, X. Zhou, B. Li, and C. Zhang, "Recent progress of the gas diffusion layer in proton exchange membrane fuel cells: Material and structure designs of microporous layer," *Int. J. Hydrogen Energy*, vol. 46, no. 5, pp. 4259–4282, 2021.
[39] Y. Wang, S. J. Moura, S. G. Advani, and A. K. Prasad, "Power management system for a fuel cell/battery hybrid vehicle incorporating fuel cell and battery degradation," *Int. J. Hydrogen Energy*, vol. 44, pp. 8479–8492, 2019.
[40] X. Hu, C. Zou, X. Tang, T. Liu, and L. Hu, "Cost-optimal energy management of hybrid electric vehicles using fuel cell/battery health-aware predictive control," *IEEE Trans. Power Electron.*, vol. 35, no. 1, pp. 382–392, Jan. 2020.
[41] T. Flecher, R. Thring, and M. Watkinson, "An energy management strategy to concurrently optimise fuel consumption & PEM fuel cell lifetime in a hybrid vehicle," *Int. J. Hydrogen Energy*, vol. 41, no. 46, pp. 21503–21515, 2016.
[42] X. Zhang, Y. Rui, Z. Tong, X. Sichuan, S. Yong, and N. Huaisheng, "The characteristics of voltage degradation of a proton exchange membrane fuel cell under a road operating environment," *Int. J. Hydrogen Energy*, vol. 39, no. 17, pp. 9420–9429, 2014.
[43] H. Chen, P. Pei, and M. Song, "Lifetime prediction and the economic lifetime of proton exchagne membrane fuel cells," *Appl. Energy*, vol. 142, pp. 154–163, 2015.
[44] C. Dépature *et al.*, "IEEE VTS motor vehicles challenge 2017 - energy management of a fuel cell/battery vehicle," in *Proc. IEEE Veh. Power Propulsion Conf.*, 2016, pp. 4635–4640.
[45] K. Davis and J. G. Hayes, "Fuel cell vehicle energy management strategy based on the cost of ownership," *IET Elect. Syst. Transp.*, vol. 9, no. 4, pp. 226–236, 2019.
[46] S. Wei *et al.*, "Optimisation of a catenary-free tramline equipped with stationary energy storage systems," *IEEE Trans. Veh. Technol.*, vol. 69, no. 3, pp. 2449–2462, Mar. 2020.
[47] N. Murgovski, L. J. Mårdh, A. Grauers, and J. Sjöberg, "Dimensioning and control of a thermally constrained double buffer plug-in hev powertrain," in *Proc. IEEE 51st IEEE Conf. Decis. Control*, 2012, pp. 6346–6351.
[48] N. Murgovski, L. M. Johannesson, and B. Egardt, "Optimal battery dimensioning and control of a CVT PHEV powertrain," *IEEE Trans. Veh. Technol.*, vol. 63, no. 5, pp. 2151–2161, Jun. 2014.
[49] H. Liimatainen, M. Pöllänen, and L. Nykänen, "Impacts of increasing maximum truck weight - case Finland," *Eur. Transport Res. Rev.*, vol. 12, no. 1, 2020.
[50] N. Murgovski, L. Johannessona, J. Sjöberg, and B. Egardta, "Component sizing of a plug-in hybrid electric powertrain via convex optimization," *Mechatronics*, vol. 12, no. 1, pp. 106–120, 2017.
[51] L. Johannesson, N. Murgovski, S. Ebbesen, B. Egardt, E. Gelso, and J. Hellgren, "Including a battery state of health model in the HEV component sizing and optimal control problem," *Int. Federation Accountants Proc. Volumes*, vol. 46, no. 21, pp. 398–403, 2013.
[52] N. Murgovski, X. Hu, L. Johannesson, and B. Egardt, "Filtering driving cycles for assessment of electrified vehicles," in *Proc. Workshop New Energy Veh. Dyn. Syst. Control Technol.*, 2013.
[53] N. Murgovski, L. Johannesson, J. Hellgren, B. Egardt, and J. Sjöberg, "Convex optimization of charging infrastructure design and component sizing of a plug-in series HEV powertrain," *Int. Federation Accountants Proc. Volumes*, vol. 44, no. 1, pp. 13052–13057, 2011.
[54] S. Boyd and L. Vandenberghe, *Convex Optimization*. Cambridge, U.K.: Cambridge Univ. Press, 2004.
[55] G. Glenk and S. Reichelstein, "Economics of converting renewable power to hydrogen," *Nature Energy*, vol. 4, pp. 212–216, 2019.

Qian Xun (Graduate Student Member, IEEE) received the B.Eng. degree from Hohai University, Nanjing, China, in 2012, and the M.Sc. degree from the Nanjing University of Aeronautics and Astronautics, Nanjing, China, in 2015. She is currently working toward the Ph.D. degree with the Chalmers University of Technology, Gothenburg, Sweden. She was a Lecturer with Huzhou University, China, for two years. Her research interests include modeling, control, and optimization of fuel cell hybrid electric vehicles.

Nikolce Murgovski received the M.S. degree in software engineering from University West, Trollhattan, Sweden, in 2007, the M.S. degree in applied physics and the Ph.D. degree in systems and control from the Chalmers University of Technology, Gothenburg, Sweden, in 2007 and 2012, respectively. He is currently an Associate Professor with the Department of Electrical Engineering, Chalmers University of Technology. His research interests include optimization and optimal control in the automotive area.

Yujing Liu (Senior Member, IEEE) received the B.Sc., M.Sc., and Ph.D. degrees in electrical engineering from the Harbin Institute of Technology, Harbin, China, in 1982, 1985, and 1988, respectively. From 1996 to 2013, he was with ABB Corporate Research, Västeras, Sweden. Since 2013, he has been a Professor of Electric Power Engineering with the Chalmers University of Technology, Gothenburg, Sweden. He is a Member of the Swedish Standard Committee on Electrical Machines. His research interests include motors, converters, wireless charging for electric vehicles, generators, and power electronics for tidal power conversion, and high-efficiency machines for energy saving in industrial applications.